HYDROTHERMAL SYNTHESIS AND STRUCTURAL CHARACTERIZATION OF OPEN-FRAMEWORK METAL PHOSPHATES TEMPLATED WITH ORGANIC DIAMINES

A Thesis Submitted to
the Graduate School of Engineering and Sciences of
İzmir Institute of Technology
in Partial Fulfillment of the Requirements for the Degree of

MASTER OF SCIENCE

in Chemistry

by
Özlem ECE

July 2012
İZMİR

We approve the thesis of **Özlem ECE**

Examining Committee Members:

_____

Assoc. Prof. Dr. Mehtap EANES
Department of Chemistry, İzmir Institute of Technology

_____

Assoc. Prof. Dr. Funda DEMİRHAN
Department of Chemistry, Celal Bayar University

_____

Inst. Dr. Saliha Nigar ŞERBETÇİOĞLU
Department of Chemistry, İzmir Institute of Technology

9 July 2012

_____

Assoc. Prof. Dr. Mehtap EANES
Supervisor, Department of Chemistry
İzmir Institute of Technology

_____

Prof. Dr. Durmuş ÖZDEMİR
Head of the Department of Chemistry

_____

Prof. Dr. R. Tuğrul SENGER
Dean of the Graduate School of Engineering and Sciences

ACKNOWLEDGEMENTS

I would like to extend my special appreciation to my research advisor, Assoc. Prof. Dr. Mehtap EMİRDAĞ EANES for her support, endless patience and guidance through my master thesis.

Special thanks to my friend Banu ÖNEN for her all help, support and friendship through my master.

Next, I wish to express my thanks to all my friends at IZTECH especially Nesrin HORZUM POLAT, Özge TÜNCEL, Seçil SEVİM, Gülçin ÜNAL, Taylan MEŞİN, Mithat BOZ and all my laboratory mates.

I also wish to express my thanks to Deniz ÇELİK, Esra KUDAY, Duygu VURAL and Begüm AKARSU for their emotional supports.

Additionally, my deepest gratitude goes to my family, my mother Pervin ECE, my father Nafiz ECE for their endless love, understanding, encouragement, patience and support throughout my entire life.

Finally, I would like to thank Dr. Hüseyin ÖZGENER for Fourier Transform Infrared Spectroscopy (FT-IR) analysis, TÜBİTAK for their financial support, Center of Materials Research (İYTE-MAM) researches for Powder X-ray Diffraction, Scanning Electron Microscope (SEM-EDX) and thermogravimetric analyses, Clemson University for Single Crystal X-ray Diffraction analyses.

ABSTRACT

HYDROTHERMAL SYNTHESIS AND STRUCTURAL CHARACTERIZATION OF OPEN-FRAMEWORK METAL PHOSPHATES TEMPLATED WITH ORGANIC DIAMINES

In recent years, hydrothermal synthesis and structural characterization of open-framework metal phosphates templated with organic diamines have attracted the attention of scientists because they represent the interaction between organic and inorganic chemistry and can be applied in lots of branches of chemistry with their different characteristic properties.

In this study, a novel open-framework polyoxometal phosphate compound $(4,4'\text{-bpyH}_2)_2(4,4'\text{-bpyH})[PCoW_{11}O_{39}].H_2O$ was synthesized with hydrothermal method as red crystals. The compound crystallizes in the space group P2(1)/n of the monoclinic system with four formula units in a cell. The crystal is a Keggin polyoxometalate structure and contains free 4,4'-bipyridine groups and water molecule between the clusters.

In addition to this novel compound, three known compounds were synthesized. $Co(4,4'\text{-bpy})_2(VO_2)_2(HPO_4)_2$ red crystals were synthesized hydrothermally and the compound crystallizes in the space group C2/c of the monoclinic system with four formula units in a cell. The crystal consists of $[(VO_2)(HPO_4)]_\infty$ helical chains and $[Co(4,4'\text{-bpy})_2]^{2+}$ frameworks.

Also, $NaCo_3(PO_4)(HPO_4)_2$ pink crystals were obtained with using hydrothermal synthesis. The compound crystallizes in the space group C2/c of the monoclinic system with four formula units in a cell. In the structure, CoO_6 chains connect to the PO_4 and HPO_4 groups.

Lastly, $(enH_2)_3[CoW_4P_4O_{28}]$ blue crystals were synthesized with hydrothermal method and crystallizes in the space group I4(1)/a of the tetragonal system with four formula units in a cell. The crystal consists of a $[Co_3W_4P_4O_{28}]^{6-}$ anion and three free ethylenediaminium $(N_2H_{10}C_2)^{2+}$ cations.

ÖZET

ORGANODİAMİN GRUPLARIYLA ŞEKİLLENDİRİLEN AÇIK KRİSTAL YAPILI METAL FOSFATLARIN HİDROTERMAL SENTEZİ VE YAPISAL KARAKTERİZASYONU

Son yıllarda, hidrotermal yöntem ile sentezlenen ve yapısal karakterizasyonları gerçekleştirilen organodiamin gruplarıyla şekillendirilmiş açık kristal yapılı metal fosfat bileşiklerinin, organik ile anorganik kimyayı ilişkilendirebilmesi ve kimyanın birçok alanında kullanılabilir olması bilim adamlarının dikkatini çekmektedir.

Bu çalışmada, yeni bir açık kristal yapılı polioksometal fosfat bileşiği olan $(4,4'\text{-bpyH}_2)_2(4,4'\text{-bpyH})[PCoW_{11}O_{39}].H_2O$ kırmızı kristalleri hidrotermal yöntem ile sentezlenmiştir. Bileşik, monoklinik sistemin P2(1)/n uzay grubunda olup, dört formül birimi içeren birim hücrede kristallenmiştir. Kristal, polioksometal yapısına sahiptir ve kristalin yapısındaki su ve 4,4'-bipiridin grupları, $[PCoW_{11}O_{39}]^{5-}$ kümelerinin arasında serbest halde bulunmaktadır.

Yapılan çalışmada, yeni madde dışında üç adet bilinen kristal de sentezlenmiştir. $Co(4,4'\text{-bpy})_2(VO_2)_2(HPO_4)_2$ kırmızı kristalleri, hidrotermal yöntemle sentezlenmiştir ve bileşik monoklinik sistemin C2/c uzay grubunda olup, dört formül birimi içeren birim hücrede kristallenmiştir. Kristal, $[(VO_2)(HPO_4)]_\infty$ sarmal zincirleri ve $[Co(4,4'\text{-bpy})_2]^{2+}$ yapılarından oluşmaktadır.

Ayrıca, hidrotermal metotla sentezlenen $NaCo_3(PO_4)(HPO_4)_2$ pembe kristalleri, monoklinik sistemin C2/c uzay grubunda olup, dört formül birimi içeren birim hücrede kristallenmiştir. CoO_6 zincirleri, PO_4 ve HPO_4 gruplarıyla bağ yaparak kristal yapıyı oluşturmaktadır.

Son olarak, hidrotermal metotla sentezlenen $(enH_2)_3[CoW_4P_4O_{28}]$ koyu mavi kristalleri ise, tetragonal sistemin I4(1)/a uzay grubunda olup, dört formül birimi içeren birim hücrede kristallenmiştir. Kristal, bir adet $[Co_3W_4P_4O_{28}]^{6-}$ anyonu ve üç adet serbest etilendiaminyum $(N_2H_{10}C_2)^{2+}$ katyonlarından meydana gelmektedir.

TABLE OF CONTENTS

LIST OF FIGURES

Figure **Page**

LIST OF TABLES

Table **Page**

CHAPTER 1

INTRODUCTION

Solid state chemistry deals with synthesis, structure, properties and applications of solid materials and these materials are generally inorganic. Organic solids are also included since they present interesting physical properties like high electrical property and the reactions of organic solids are connected to topochemical control. For example, they are influenced by their molecular packing arrangement. Therefore, minerals are included because they are examples of inorganic solids which occur in nature.

Most of the inorganic solids are non-molecular and their structure is determined by the manner in which atoms or ions are packed together in three dimensions. Their various and complex structure types are the center of appreciation of solid state chemistry. This includes description and classification of crystal structures by the knowledge of space groups and estimation of the factors which affect and control the crystal structures.

An important structural aspect is the defect structure of solids. These defects have a great effect on properties just as mechanical strength, electrical conductivity and chemical reactivity. These allow the various composition of solids in the framework of the same overall crystal structure. Thus, it is possible to control or modify many properties by changing the compositions.

There are several methods in order to synthesize solids. These are vapour phase transport, precipitation, electrochemical methods, ceramic methods, solvothermal and hydrothermal methods (West, 1984).

The purpose of this study is to gain open-framework metal phosphates which are composed of transition metal oxides (V, W) and organic diamines interacted with the inorganic part of these materials.

Hydrothermal synthesis method is chosen to synthesize organic-inorganic hybrid materials since the other solid state synthesis methods are usually carried out by high temperature (1000°C) solid-solid interactions and this method is powerful in order to produce stable organic-inorganic hybrid materials.

1.1. Hydrothermal Synthesis

Hydrothermal synthesis method is finding increasing applications in materials science and solid state chemistry. It is a technologically important method for crystal growth and the synthesis of new materials with useful properties. It is also interesting scientifically because using high pressure provides an additional parameter for obtaining fundamental information on the structures, behaviour and properties of solids.

Hydrothermal synthesis is a chemical reaction in the presence of aqueous solvents above 100˚C and at pressures greater than 1 atm in a closed system in order to dissolve and recrystallize materials which are relatively insoluble under normal conditions.

In 1913, hydrothermal method described by Morey and Niggli as a method in which the components are subjected to the action of water, at temperatures are usually above the critical temperature of water (370°C) in closed bombs, and therefore, under the corresponding high pressures developed by such solutions.

Also, according to Yoshimura (1974), hydrothermal reactions occur under the conditions of high temperatures and high pressures (>100°C, >1 atm) in aqueous solutions and in a closed system.

Although most of the scientists think that hydrothermal synthesis carries out above 100°C temperature and above 1 atm pressure, there is no definite lower limit for temperature and pressure conditions (Byrappa and Yoshimura, 2001).

Hydrothermal reaction is generally chosen for the;

- Synthesis or stabilization of new compounds
- Growth of single crystals
- Preparation of finely divided materials and microcrystallites which have well-defined size and morphology
- Filtration of ores in metal extraction
- Decomposition, modification, corrosion, etching

Water is used as catalyst or sometimes it is used as a component of solid phases in hydrothermal synthesis. The critical temperature and pressure of water are 374°C and 22.1 MPa and the solvent properties for supercritical water (dielectric constant and solubility) changes rather than the properties of water under normal conditions which is shown in Figure 1.1.

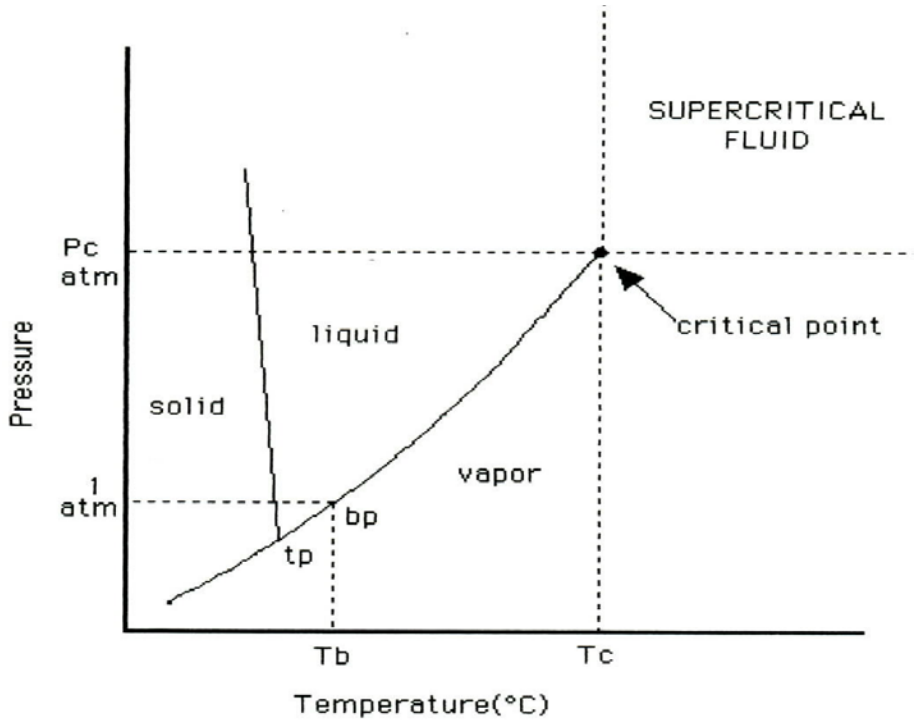

Figure 1.1. Phase Diagram of Water.
(Source: Eral, 2006)

The dielectric constant of water is 78 at room temperature, so polar inorganic salts can be soluble in water at this temperature. The density and dielectric constant of water decrease when temperature increases and pressure decreases as shown in Figure 1.2. The dielectric constant of supercritical water is below 10, so the addition of the dielectric constant to the reaction rates becomes remarkable in terms of the electrostatic theory. So that, a favorable reaction field for particle formation was given by water under supercritical conditions, in view of increasing of the reaction rate and large supersaturation based on the nucleation theory, because the solubility is getting lower. Supercritical water has specific properties encouraging low solubility of inorganics but high solubility of organics, because of its low dielectric constant, that makes it suitable for the synthesis of hybrid particles (Hayashi and Hakuta, 2010).

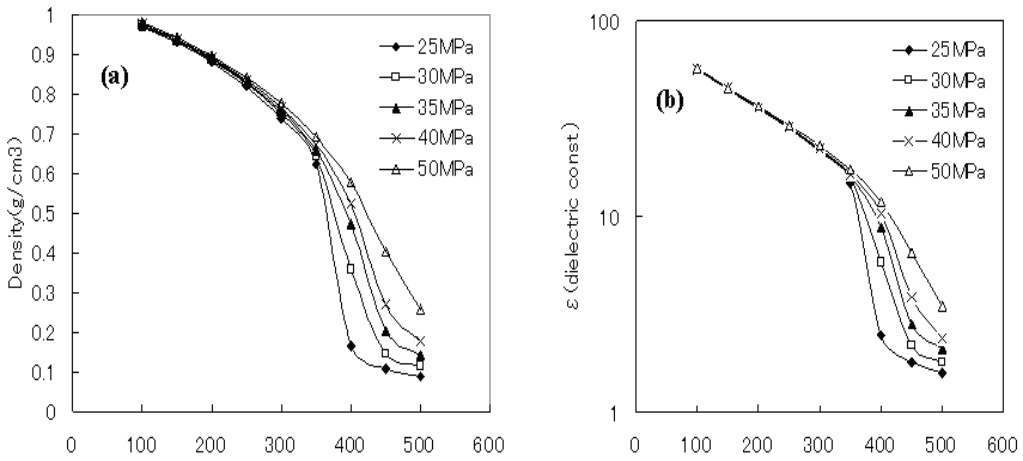

Figure 1.2. (a) Density of water as a function of temperature and pressure. (b) Dielectric constant as a function of temperature and pressure. (Source: Hayashi and Hakuta, 2010)

On the other hand, the viscosity of supercritical water decreases and causes the mobility to increase and diffusion processes to become easier at high temperatures and pressures. The low viscosity and high mobility of supercritical water make it a suitable medium for preparing metastable phases and single crystals that have good quality (Byrappa and Yoshimura, 2001).

Also, hydrothermal reaction does not need much time compared to traditional methods. Although a solid state reaction can be done in a few weeks, hydrothermal reaction can be performed in a few days.

Hydrothermal synthesis takes place in closed vessel whose pressure is determined by the temperature and the degree of filling in most of the experiments. Hydrothermal crystallization is made possible with the vessel filled to 32% total volume and more successfully above 65% with pressures of 200-3000 bar which are shown in Figure 1.3.

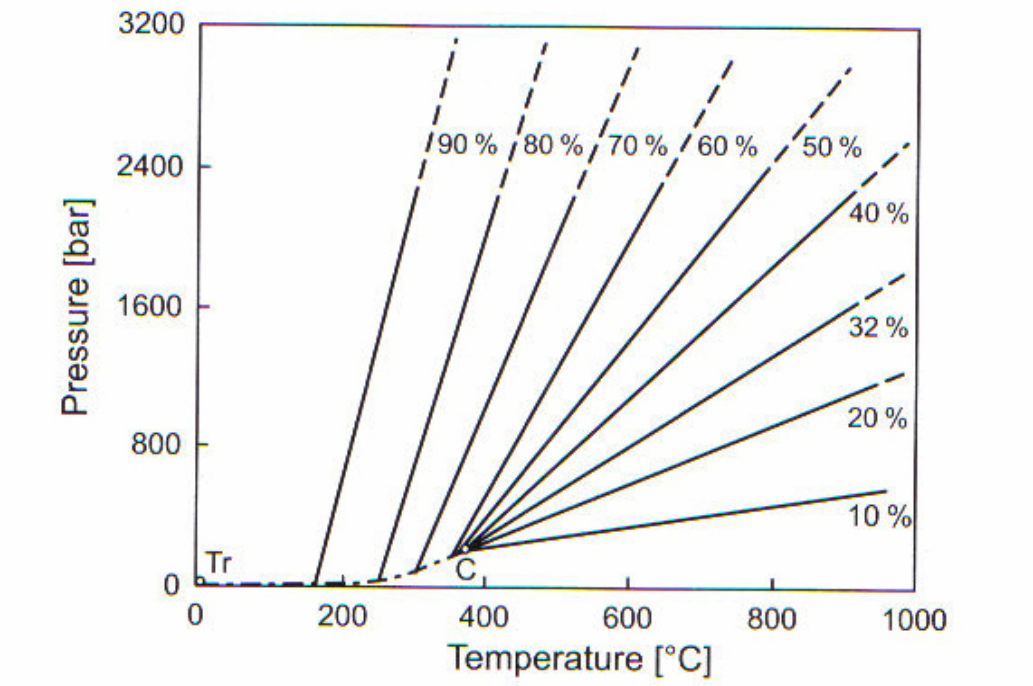

Figure 1.3. Pressure/temperature relation of water for different degrees of reaction vessel filling. (Source: Schubert and Hüsing, 2005)

1.1.1. History of Hydrothermal Synthesis

The term 'hydrothermal' was first used by British Geologist Sir Roderick Murchison (1792-1871) in order to explain the behavior of water at high temperature and pressure in the formation of various rocks and minerals with the changes in the earth's crust. Hydrothermal technique was then used by Bunsen (1845) by using thick walled glass tubes to contain high temperature and pressure liquids and prepared barium and strontium carbonates. Wohler (1848) used hydrothermal technique to recrystallize appophyllite by heating in water solutions at 180-190°C and 10-12 atm. Hydrothermal experiments were carried out generally in simple glass tubes until 1881. Daurree (1857) first used a steel tube in order to synthesize quartz and wollastonite at 400°C by using water as a solvent.

The first successful application of the hydrothermal synthesis was the mineral extraction in 1892 by Karl Josef Bayer (1871-1908). Then, large single crystals of quartz were synthesized by Nacken (1946) and zeolites were synthesized by Barrer (1948).

During the World War II, hydrothermal synthesis was used in many laboratories in Europe and North America for the growth of large size crystals. Through the 19th century; Germany, France, Italy and Switzerland; also, through the 20th century; USA, Soviet Union and Japan are the major centers for the development of hydrothermal technology.

During the last fifteen years, hydrothermal synthesis has been the most popular technique for the scientist of different disciplines (Byrappa and Yoshimura, 2001).

1.2. Organic-Inorganic Hybrid Materials

Organic-inorganic hybrid materials represent the interaction between the two major branches of chemistry (organic and inorganic chemistry). Each of these branches importantly contributes to the materials science and have characteristic properties that induce various advantages and limitations. The most commonly used definition of these materials is the following; 'a hybrid material is a material that includes two moieties blended on the molecular scale. Commonly one of these compounds is inorganic and the other one organic in nature.' The reason for developing hybrid materials is to take the best properties of each component while eliminating their particular limitations and produce new materials with new properties.

Although the original birth of hybrid materials are not known exactly, the mixing of organic and inorganic components was carried out in ancient world, but at the end of the 20th and at the beginning of 21st century, hybrid materials attracted scientists attention because of their availability of novel physico-chemical characterization methods and the field of nanoscience opened many points of view for approaches to new materials.

Organic-inorganic hybrid materials are simple to process and suitable to design on the molecular scale, so they can be applied in lots of branches of materials chemistry with their different mechanical and characteristic properties. Chemical activity is the main property of hybrid materials. They bind the chemical activity of their constituents by exploring their ionic conductivity, selectivity, luminesence, electrical and optical properties, chemical or biochemical activity which are used in selective membranes, batteries, sensors, electrochemical devices, electrochemical supercapacitors, supported catalysts and photochemical energy conversion cells.

Hybrid materials can be classified by using their field of application or their chemical nature. Firstly, P. Judenstein et al. classified the hybrid materials based on the interactions between the organic and inorganic interphase and the selected interactions are illustrated in Figure 1.4. This classification has two types;

Type1: Weak interactions between two phases, Van der Waals, H-bonding or weak electrostatic interactions.

Type2: Strong chemical interactions between the components.

Although this is a simple classification, it helps the first prediction to categorize the complication of a wide variety of systems (Kickelbick, 2007).

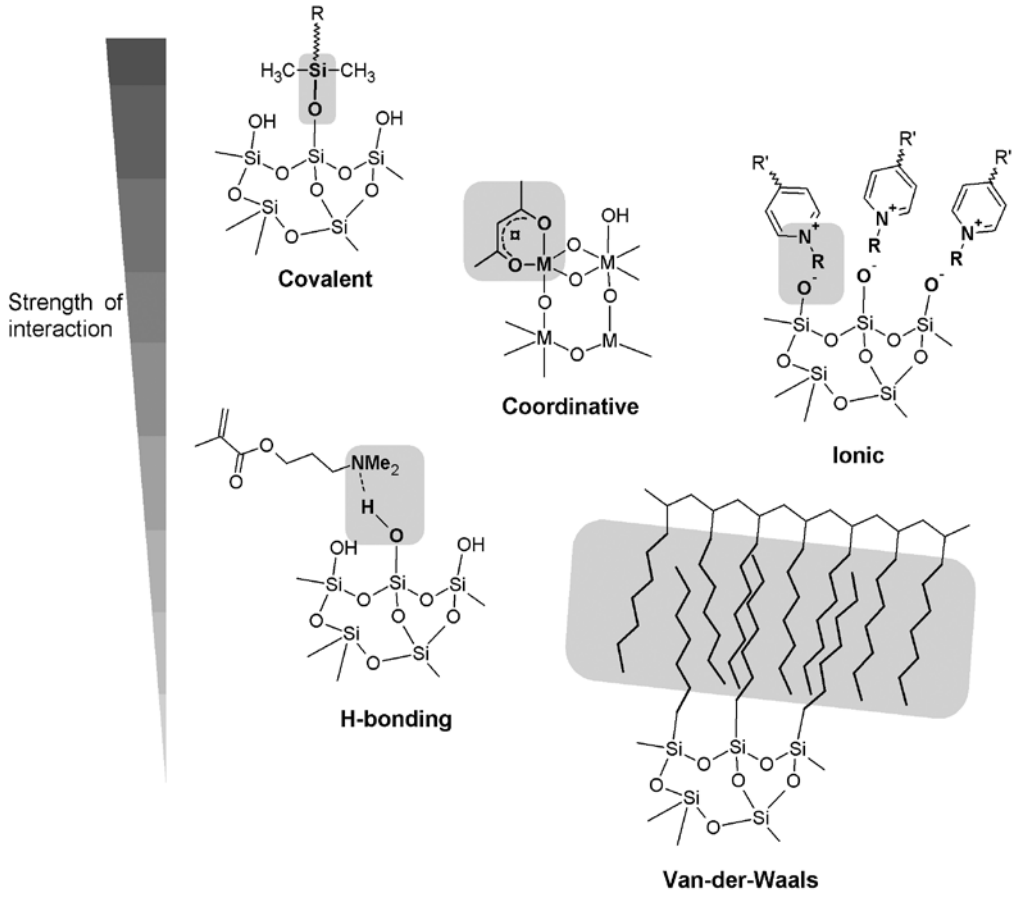

Figure 1.4. Selected interactions typically applied in hybrid materials and their relative strength. (Source: Kickelbick, 2007)

Hybrid materials include a wide range of organic and inorganic parts. Generally inorganic part involves transition metal oxides or p-block elements and organic part involves organic diamine ligands. Organic component can affect the microstructures of

inorganic oxide part by controlling the nucleation and growth of the inorganic oxide. There is a synergistic interaction between these two parts of hybrid materials. This gives the information about organic and inorganic structures. Additionally, more complex phases can be produced by a shift from thermodynamic to kinetic domain rather than equilibrium phases and secondary metal complexes are used to cause more complex structures. These secondary metal complexes make bridges between the metal oxide and organic component that cannot bond directly to metal oxide.

There are various modes of involvement of organonitrogen components in metal oxide structures. These are space filling, structure directing, charge compensating, ligand bound to a secondary metal site (M'), ligand bound directly to the metal oxide structure which are illustrated in Figure 1.5.

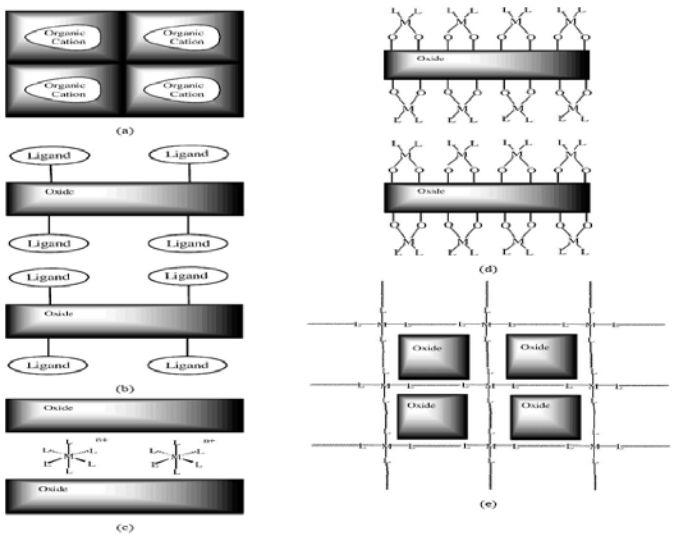

Figure 1.5. Different functions of organonitrogen component; a) charge compensating cation, b) ligand bound directly to metal oxide structure, c) ligand bound to a secondary metal site (M'), d) ligand that is on secondary metal bounded to the metal oxide structure, e) briging ligand between the secondary metal complexes. (Source: Hagrman et al., 1999)

CHAPTER 2

EXPERIMENTAL METHOD

2.1. Autoclaves

Crystal synthesis and growth under hydrothermal conditions requires a pressure vessel that is capable of containing highly corrosive solvent at high temperature and pressure. This suitable or ideal hydrothermal apparatus is 'autoclave' (Xu et al., 2010).

The first autoclave was made in Europe alone in the 19th century and used worldwide in the 20th century. An ideal autoclave for hydrothermal synthesis should include the following characteristics;

- Inertness to oxidizing agents, acids and bases
- Easy to operate and maintain
- A suitable size and shape to obtain a desired temperature gradient
- Leak-proof with unlimited capabilities to the required pressure and temperature
- High mechanical strength to bear high pressure and temperature experiments for long duration

The most successful materials for autoclaves are corrosion resistant, high-strength alloys such as stainless steel, iron, nickel, cobalt based super alloys and titanium and its alloys. In some hydrothermal reactions, the reagents and solvents are noncorrosive and the reactions can take place in autoclaves directly. However, in most of the hydrothermal experiments, the reagents and solvents are corrosive and they can attack the vessel in high temperatures and pressures. Thus, it requires a suitable lining for the inner wall of the autoclave. In order to grow high purity crystals in highly corrosive environment, teflon beakers or liners are used. The teflon liner or beaker should sit exactly inside the autoclave without leaving any space. Teflon is the most popularly used lining material but it cannot be used at more than 300˚C because teflon dissociates affecting the pH of unbuffered, near-neutral solutions above this temperature (Byrappa and Yoshimura, 2001). Figure 2.1 illustrates a stainless steel autoclave and its parts which were used in this study.

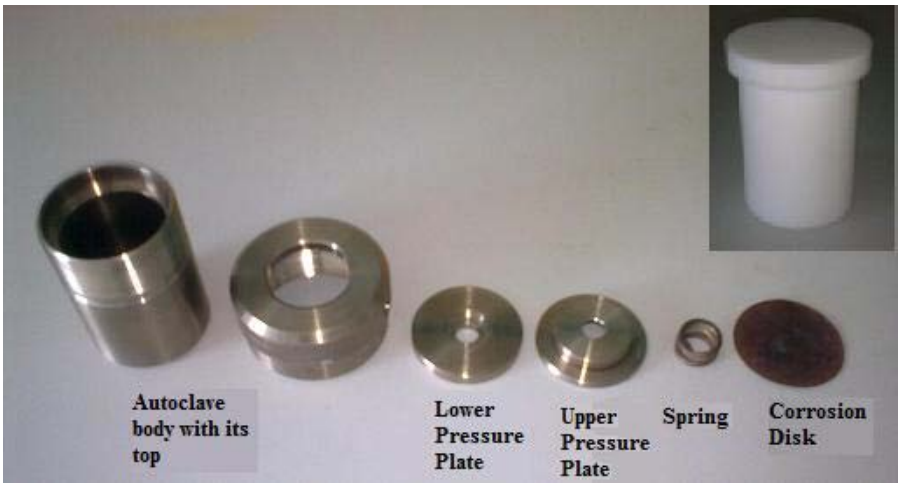

Figure 2.1. Steel autoclave and Teflon vessel.
(Source: Kepenekci et al., 2011)

2.2. Hydrothermal Procedure

Hydrothermal reactions take place in steel autoclaves, inside of which have Teflon vessels (23 ml) between 100-250˚C. Teflon is an inert material, so it does not go into reaction with the starting materials. First of all, teflon vessels are filled with starting materials (transition metal oxide, organic component, secondary metal salt, phosphoric acid) and reaction solution (water). To provide enough pressure, minimum 50% of the reaction cup is filled with the solvent. Then, teflon vessels are placed in steel autoclaves and put in an oven. Above 100˚C, water is vaporized and solves the initial compounds that could not be solved easily in normal conditions. After reaching the temperature that we want, reactions are kept 2, 3 or 4 days at this temperature. After the end of this period, reaction cups are cooled slowly to room temperature. Crystals that have best quality and size are formed in this cooling period. After that, products are filtered by vacuum filtration and washed several times with pure water in order to remove the traces of solvent from the products. If the crystals are observed under the optical microscope, they are analyzed with Powder X-ray Diffractometer, spectroscopic techniques, Scanning Electron Microscope-EDX, Single Crystal X-ray Diffractometer and their structures are determined by using ShelXTL (crystal structure program).

2.3. Characterization of Crystals

There are three main techniques to characterize the crystalline materials. These main techniques are diffraction, microscopic and spectroscopic techniques. In addition to these, thermogravimetric analysis method is used to have an opinion for components of the crystals.

2.3.1. Diffraction Techniques

Diffraction techniques are used to solve the structure of crystals. They determine the precise atomic positions, the bond lengths and angles of molecules within a single crystal.

There are three types of radiation used for crystal diffraction studies; X-rays, electrons and neutrons that are mentioned above. Among these, X-rays radiation is the most common radiation type but electron and neutron diffractions have significant specific applications.

2.3.1.1. X-ray Diffraction

Certainly, X-ray diffraction is the most important and beneficial technique in solid state chemistry and it has been applied for the fingerprint characterization of crystals and for the determination of their structures. This method requires an X-ray source (monochromatic or of variable λ), the sample (single crystal, powder or solid piece) which is under investigation and a detector (radiation counter or photographic film) that takes the diffracted X-rays.

X-rays are electromagnetic radiation of wavelength ~1 Å (10^{-10} m). They occur between γ-rays and the ultraviolet part of the electromagnetic spectrum (Figure 2.2).

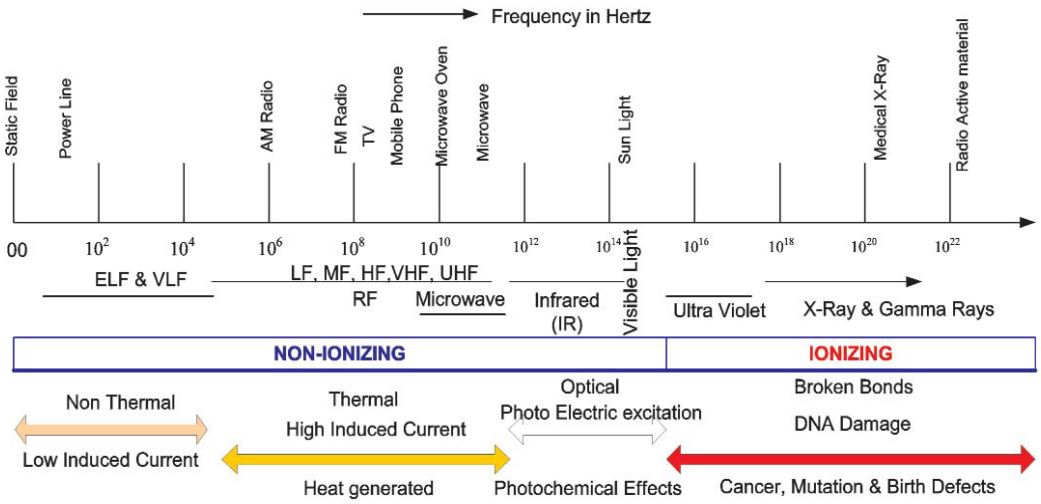

Figure 2.2. Electromagnetic spectrum of light.
(Source: Zamanian and Hardiman, 2005)

X-rays are generated when high energy changed particles, e.g. electrons, accelerated through 30000 V, collide with matter. The electrons are decelerated by the collision and some of their lost energy is transformed into electromagnetic radiation. Such processes give ‘white radiation’, X-rays which have wavelengths ranging upwards from a significant lower limiting value. This lower wavelength limit corresponds to the X-rays of the highest energy and takes place when all the kinetic energy of the incident particles is changed into X-rays.

The X-rays which are preferred for generally all diffraction experiments are produced by a different process that causes monochromatic X-rays. A beam of accelerated electrons is allowed to strike a metal target, often copper. The incident electrons have enough energy in order to ionize some of the copper 1s (K shell) electrons. An electron in an outer orbital (2p or 3p) instantly goes down to occupy the vacant 1s level and the energy revealed in the transition appears as X-radiation. The transition energies have fixed values and so a spectrum of characteristic X-rays takes place.

2.3.1.1.1. Crystals and Diffraction of X-rays

Comparing with the diffraction of light by an optical grating, crystals that have regularly repeating structures, should diffract radiation which has a wavelength like interatomic separation ~ 1 Å.

The X-ray wavelength commonly employed is the characteristic Kα radiation, $\lambda = 1.5418$ Å, emitted by copper.

When crystals diffract X-rays, atoms or ions act as secondary point sources and scatter the X-rays; in the optical grating it is the lines scratched or ruled on the glass surface that lead to scattering.

Throughout history, two approaches have been used to treat diffraction by crystals; The Laue Equations and Bragg's Law. The Laue method is mostly used to determine the orientation of large single crystals. White radiation is reflected from, or transmitted through, a fixed crystal.

The diffracted beams form arrays of spots, that lie on curves on the film. The Bragg angle is fixed for every set of planes in the crystal. Each set of planes picks out and diffracts the particular wavelength from the white radiation that satisfies the Bragg's Law (Regard crystals as built up in layers or planes such that each acts as a semi-transparent mirror. The angle of reflection is equal to the angle of incidence) for the values of d and θ involved. Each curve therefore corresponds to a different wavelength. The spots lying on any one curve are reflections from planes belonging to one zone (Figure 2.3).

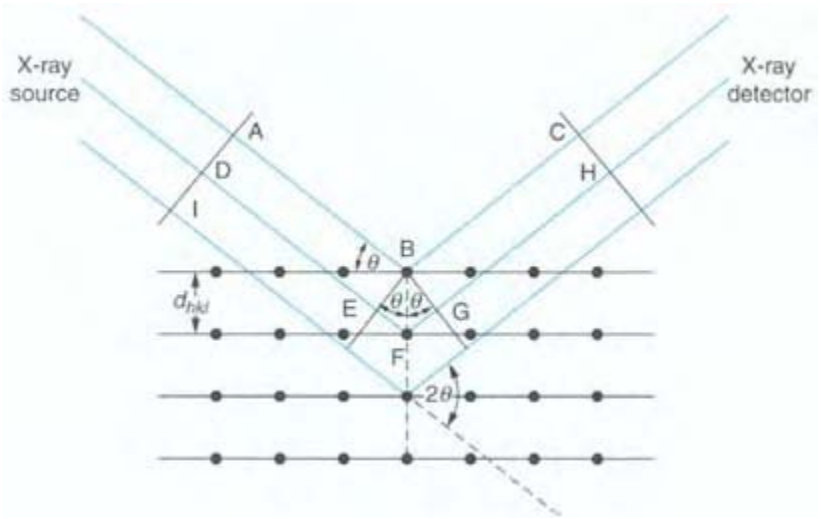

Figure 2.3. Schematic representation of Bragg reflection from a set of crystal planes with a spacing d_{hkl}. (Source: Smart and Moore, 2005)

Laue reflections from planes of same zone all lie on the surface of an imaginary cone whose axis is the zone axis. Crystal orientation is determined from the position of the spots.

The Laue technique can also be used to estimate crystal perfection from the size and shape of the spots. If crystal has been bent or twisted in anyway, the spots become deformed and smeared out (Smart and Moore, 2005).

2.3.1.1.2. Powder X-ray Diffraction

Powder X-ray diffraction is a non-destructive analyzing method on behalf of determining chemical and physical characteristics of materials. It is commonly preferred in all fields of science and technology. Applications of this method are; crystallographic unit cell and crystal structure, crystalline size, crystallographic texture, phase analysis, microstrain and macro-stress, electron radial distribution functions. The most important application of the powder X-ray diffraction method is the qualitative identification of crystalline phases or compounds.

The term ‘powder’, that is used in powder diffraction, does not certainly mean the usual sense in the word in common language. In powder diffraction method, the sample can be a ‘solid substance which is divided into very small particles’. Besides

that, it can be a solid block like a metal, ceramic, polymer, glass, thin film or liquid. The reason is that the important parameters are the number and size of the individual crystals in the sample in order to define the concept of a powder for a diffraction experiment. It is not related to their growing degree.

An ‘ideal’ powder that is used in diffraction method includes a large number of a randomly oriented small crystals. A large number means that there are always enough crystals in any diffracting orientation for giving reproducible diffraction patterns. The crystal size must be small due to the characteristics of the sample and the diffraction geometry in order to get a precise measurement of the intensity of diffracted rays.

A monochromatic beam of X-rays collides with the powdered sample that contains crystals arbitrarily arranged in every possible orientation in powder X-ray diffraction. Therefore, some crystals must be oriented at the Bragg angle, θ, to the incident beam for each set of planes, so that diffraction occurs for these crystals and planes. The diffracted beams can be detected not only by surrounding the sample with a strip of photographic film but also by using a movable detector, such as Geiger counter, which is connected to a diffractometer that is a chart recorder (Figure 2.4).

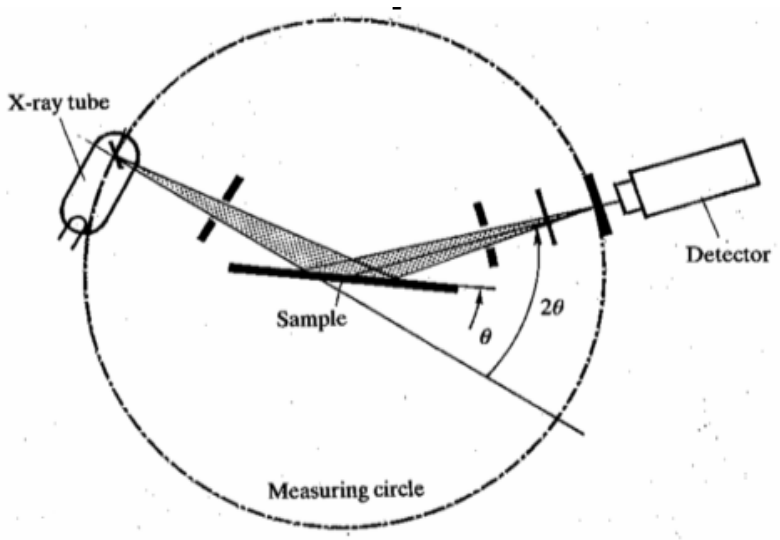

Figure 2.4. The X-ray Spectrometer.
(Source: Smart and Moore, 2005)

Although most of the chemical methods of analysis give information about the elements present in a sample, powder diffraction is a common method to tell which crystalline compounds or phases present but it does not give any direct information about their chemical composition. Each crystal has a typical powder pattern that is used as a fingerprint for identification purposes. Peak position and intensity are the two variables in powder pattern.

In order to identify the unknown crystals, an invaluable reference source is the Powder Diffraction File (Joint Committee on Powder Diffraction Standarts, USA), previously known as ASTM file, which includes the powder patterns of about 35000 materials; new entries are added at the current rate of ~ 2000 p.a. (Smart and Moore, 2005).

In the search indices, materials are classified not only according to their most intense peaks but also according to the first eight lines in the powder pattern in order of decreasing d-spacing. Identification of an unknown material is generally possible with obtaining its measured powder pattern at about 30 min (Figure 2.5). However, problems appear if the material is not included in the file or if the material is not pure but contains lines from more than one phase. The synthesized crystals were analyzed by Philiphs X'Pert Pro Powder X-ray Diffractometer.

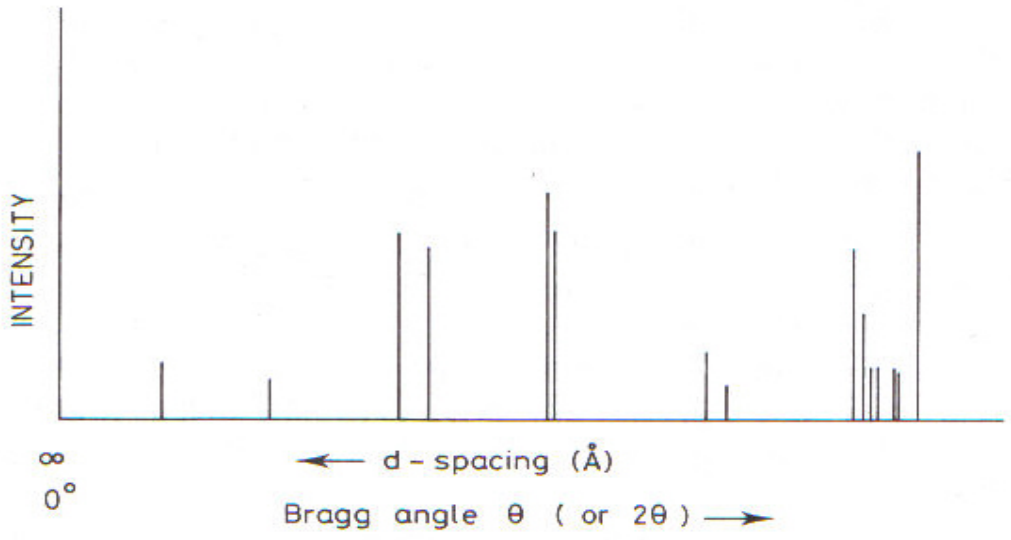

Figure 2.5. Systematic powder X-ray diffraction pattern.
(Source: West, 1984)

2.3.1.1.3. Single Crystal X-ray Diffraction

By using single crystal X-ray diffraction method, it is possible to determine a full crystal structure by measuring the position and intensity of the hkl reflections. The unit cell dimensions, space group and the precise atomic positions are also determined. Mostly, this can be done with speed and accuracy and this is one of the most powerful structural methods in chemisty (Smart and Moore, 2005).

The Bragg angle of the reflections is measured and successfully indexed, then the information on the size of the unit cell is taken and it possesses any translational symmetry elements, also on the symmetry. Additionally, the intensity of each reflection is different and this can also be measured. In modern diffractometers, the beam is picked up by a detector, either a changed coupled device (CCD) plate or a scintillation counter so that all the reflections can be collected and measured at the same time and the intensity of each reflection is recorded electronically. Intensity of each reflection changes with the weight of the related atom, heavier atoms give more intense reflections.

Single crystal X-ray diffraction data is collected using a computer controlled diffractometer, which measures the Bragg angle, θ, and the intensity, I, for each hkl reflection.

Single crystal X-ray diffraction of the resulting crystals was performed using a Rigaku AFC8S diffractometer equipped with Mo Kα (λ=0.71073 Å) radiation and a Mercury CCD area detector. Data collection and processing, including corrections for absorption and Lorentz and polarization effects were performed using the CrystalClear software package. Candidate space groups were identified based on systematic absences of the data.

2.3.2. Microscopic Techniques

Generally, in order to examine a solid sample it is better to look at it under magnification because samples which are seen to be similar may look very different under the microscope as a result of their different shapes and optical properties.

There are several microscopes and they can be divided into two groups: optical microscopes and electron microscopes.

2.3.2.1. Optical Microscopy

Optical microscopy is used to examine particles down to a few micrometers under high magnification. Optical microscopy is a cheap microscopic method and it is easy for sample preparation but a conventional optical microscope uses visible radiation (wavelength 400–700 nm) and it cannot resolve images of samples that are smaller than half the wavelength of the light. As a result, it is better to use electron microscopy for submicrometer-sized particles (West, 1984).

The synthesized crystals were observed under the J.P. Selecta Zoom Stereo Microscope that is illustrated in Figure 2.6.

Figure 2.6. J.P. Selecta Zoom Stereo Microscope.

2.3.2.2. Electron Microscopy

Electron microscopy is commonly preferred for the characterization of solids to determine the structure, morphology, crystal size and the distribution of elements. An electron microscope has a similar principle with an optical microscope. The electron beam is generated by heating a tungsten filament, and focused by magnetic fields in a

high vacuum. The numerously short wavelength of the electrons reduces resolution to 0.1 nm (Smart and Moore, 2005).

2.3.2.2.1. Scanning Electron Microscopy (SEM)

In scanning electron microscopy (SEM), it is possible to observe and characterize the heterogeneous organic and inorganic materials on a nanometer (nm) to micrometer (μm) scale. Also three-dimensional-like images of the surfaces of a very wide range of materials can be taken, so it is a very popular technique for scientists. The basic constituents of the SEM are the lens system, electron gun, electron collector, visual and photorecording cathode ray tubes (CRTs) and associated electronics (Goldstein, 2003).

In scanning electron microscope technique, the electrons from a focused beam are rastered across the surface of the material. Then, electrons reflected by the surface of the sample and emitted secondary electrons are detected in order to give the surface topography of samples like catalysts, polymers and crystals. It is a common method for examining the particle size, magnetic domains, crystal morphology, and surface defects. A wide range of magnification can be used, the best achievable one is at around 2 nm. The samples sometimes need to be coated with gold or graphite for stopping charge building up on the surface (Smart and Moore, 2005).

In electron microscopy, the elements forming the sample emit characteristic X-rays. These elements are separated by using a silicon-lithium detector, and each signal is collected, amplified and corrected for absorption and other effects, in order to give qualitative and quantitative analysis of the elements whose atomic number is greater than in the irradiated particle. This technique is known as energy dispersive analysis of X-rays (EDAX or EDX) (Smart and Moore, 2005). Figure 2.7 shows an example of EDX spectrum.

In this study, Philips XL-30S FEG Scanning Electron Microscope was used to analyze the synthesized crystals.

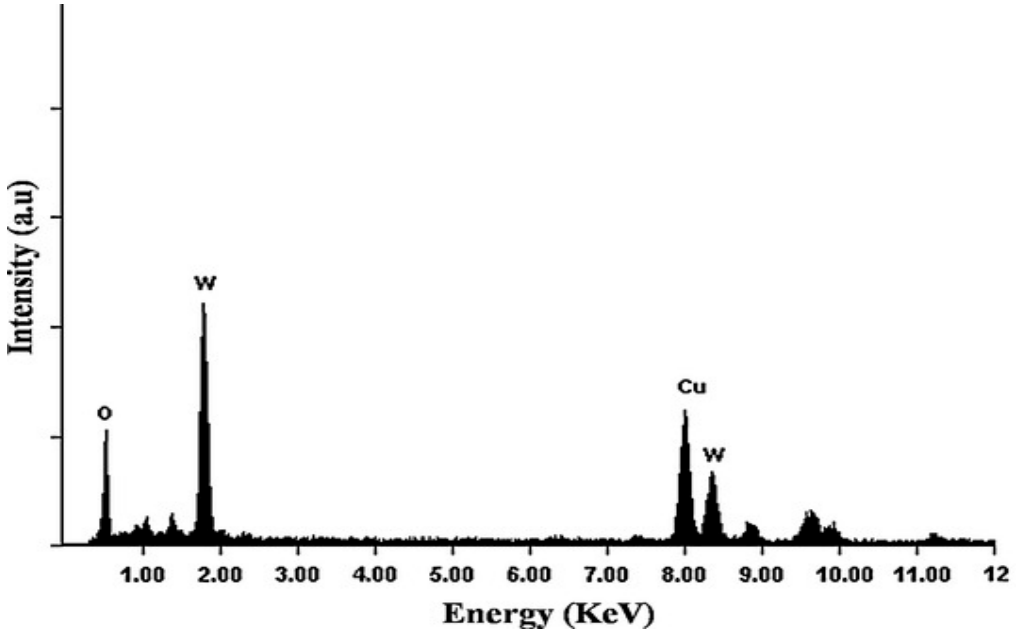

Figure 2.7. EDX spectrum of WO_3 nanorods.
(Source: Rajeswari et al., 2007)

2.3.3. Spectroscopic Techniques

Spectroscopy is an experimental technique which deals with the absorption, emission or scattering of electromagnetic radiation by atoms or molecules. There are several types of spectroscopic techniques. Some of these are vibrational spectroscopy, visible and ultraviolet spectroscopy, nuclear magnetic resonance spectroscopy, electron spin resonance spectroscopy, X-ray spectroscopies, electron spectroscopies, Mössbauer spectroscopy and mass spectrometry. All of them work on same the principle, which means materials absorb or emit energy under certain conditions.

The spectra of these techniques include X and Y axes. X axis shows the function of energy and Y axis shows the intensity of absorption or emission. The energy axis is expressed in terms of frequency, f, or wavelength, λ, of the appropriate radiation.

In this study, infrared (IR) spectroscopy, a type of vibrational spectroscopy, was used to compare the spectra of the synthesized compounds with the spectra of the compounds in literature and have an opinion about their structure and ICP-MS was used in order to have knowledge about the elements in the crystals.

2.3.3.1. Infrared Spectroscopy

In solids, atoms vibrate at frequencies of 10^{12} to 10^{13} Hz. Vibrational modes which involve groups or pairs of atoms are excited to higher energy states by absorption of radiation of appropriate frequency. IR spectrum is the plot of intensity of absorption. In IR method, the frequency of the incident radiation is diversified and the quantity of the absorbed and transmitted radiation is obtained (West, 1984).

IR spectra of solids are generally complex with a lot of peaks. Each of them shows a particular vibrational transition. A complete assignment of all peaks is possible with molecular samples and sometimes it is possible with nonmolecular samples.

Although IR spectra is mostly used for the determination of specific functional groups in organic compounds, in inorganic solids, covalently bonded linkages like hydroxyl groups, trapped water and oxyanions (carbonate, sulphate, nitrate) can give intense IR peaks (West, 1984).

The IR spectra of the synthesized crystals were taken by Perkin-Elmer Spectrum 100 FT-IR Spectrometer between 4000-400 cm^{-1}. For the analysis, KBr method was used. In this method, 1.5 mg sample was mixed with 250 mg KBr. Then, this mixture was ground by using mortar and pestle and placed inside a die. It was held in a hydraulic press for 5 minutes under 10000-psi pressure in order to form a pellet. After that, the pellet was placed inside the spectrometer port for the measurement. Sample was run in transmittance mode.

2.3.3.2. Inductively Coupled Plasma/Mass Spectrometry (ICP-MS)

Inductively coupled plasma/mass spectrometry is a common technique for elemental characterization of the materials and this tecnique has a lot of characteristics that make it significant in many analytical applications. These characteristics are; the ability of identifying and quantitative measuring of all elements in the periodic table and performing these determinations in a multielement analysis mode, measuring individual isotopes of the elements, detecting and measuring low concentrations of the elements (down to 1-10 ng of analyte element per liter in solution) and involving a large linear dynamic working range, high accuracy and precision of measurement.

The most advantageous feature of this method is using the atmospheric pressure argon inductively coupled plasma. This plasma has a high temperature (7000-10000 K). It provides exceptional atomization and atomic excitation, so it is able to analyze the materials that are difficult to atomize and difficult to excite by other atomic emission sources.

In this method, the sample (generally in aqueous solution form) is turned to an aerosol by a nebulizer and transported to the plasma by argon gas. The elements are atomized and ionized in the plasma. These ions are sampled and extracted from the plasma where they are separated and measured by a mass spectrometer (usually it is quadrupole). The ions are separated on the basis of their mass to charge ratio then a detector receives an ion signal proportional to the concentration. The concetration of the element in the sample is determined with calibration with single and multi-element reference standarts (Taylor, 2001). Agilent 7500ce Inductively Coupled Plasma/Mass Spectrometer was used to analyze the elements in the crystals.

2.3.4. Thermogravimetric Analysis

Thermal analysis is the measurement of chemical and physical properties of materials as a function of temperature and thermogravimetric analysis is one of the types of thermal analysis.

Thermogravimetry is a method in order to measure the change in weight of a substance as a function of temperature or time. The results are given as a continious chart record. In this method, a few miligrams of sample is weighed and heated at a constant rate in the range from 1 to 20˚C min^{-1}. Sample has a constant weight until it starts to decompose at initial temperature. Decomposition generally occurs over a range of temperatures, initial temperature to final temperature and a second constant weight plateau is observed above the final temperature that corresponds to the final weight of the sample. Initial weight, final weight and the difference between them are the basic properties of the sample and they are used for quantitative calculations of compositional changes. On the other hand, initial and final temperatures are based on heating rate, the nature of the solid and the atmosphere above the sample. Perkin Elmer Diamond TG/ DTA instrument was used to analyze the crystals (West, 1984).

CHAPTER 3

OPEN-FRAMEWORK METAL PHOSPHATES

In recent years, several types of inorganic open-framework structures have been synthesized and characterized. Although zeolitic aluminosilicates are the best-known open-framework structure type, open-framework metal phosphates have been gaining importance.

Open-framework metal phosphates are mostly synthesized in the presence of organic amines by using hydrothermal synthesis and they can be formed in different dimensions. These involve one-dimensional linear chains having corner-shared four-membered rings, one-dimensional ladders with edge-shared four-membered rings, two-dimensional layers, three dimensional structures with channels and zero-dimensional metal phosphate monomers including four-membered rings.

In general, four-membered rings are the simplest units in the open-frameworks and three-dimensional open-frameworks are observed more frequently than the lower dimensional ones because of their greater stability.

As aforementioned, open-framework metal phosphates mostly involve organic amines in their structures. Organic groups act as a structure directing or space-filling agent. Moreover, they can stabilize the structure through hydrogen-bonding or other interactions and help in charge compensation of the structure.

Open-framework metal phosphates have technological importance as molecular sieves, shape-selective catalysts or ion-exchange materials and the transition metal phosphates constitute an important group of them because of their potential in redox catalysis (Rao et al., 2001).

3.1. Vanadium Oxides

The vanadium element was discovered by A. M. del Rio in 1801. Later, it was rediscovered in 1830 by N. Sefström and he firstly named this element as ‘vanadium’ (after Vanadis, the Scandinavian goddess of the beauty) because of the colour richness of its compounds. Besides, vanadium is the nineteenth element which is estimated to

0.0136% of the earth's crustal rocks and also it is the fifth most abundant transition metal after iron (Fe), titanium (Ti), manganese (Mn) and zirconium (Zr). More than 60 vanadium minerals are known (Kaul, 2005).

Vanadium compounds generally have electrochemical, catalytic, magnetic and redox properties, so they are widely studied compounds. For example, bismuth oxides $BiMEVO_x$ are used for the solid electrolytes in fuel cells where as the layered lithium vanadates are used as electrodes in lithium batteries. Rather than these, some vanadates are preferred for their catalytic activities in oxidative dehydogenation of hydrocarbons and also epoxidation of olefins. Similarly, vanadium phosphates are studied for their magnetic and catalytic properties. One of the examples of them is the catalytic property of $(VO_2)P_2O_7$ in direct transforming of butane into maleic anhydride.

In mineral chemistry, vanadium atom has oxidation states from V(III) to V(V), coordinations from 6 to 4 and different environments from octahedral to tetrahedral which are illustrated in Figure 3.1. The V–O distances are given in Å.

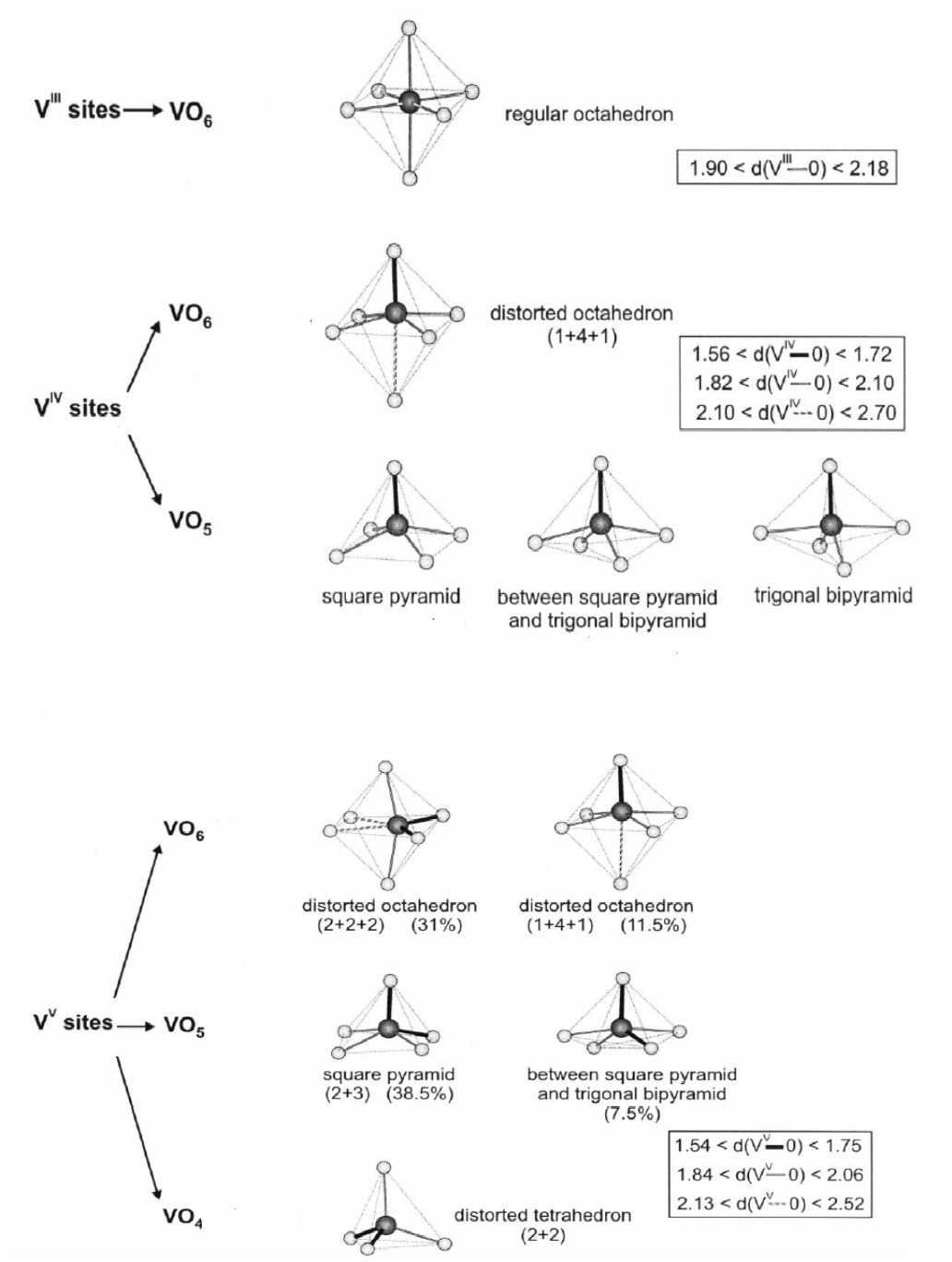

Figure 3.1. Different environments of vanadium encountered in the vanadium phosphates. (Source: Boudin et al., 2000)

.

The V^{III} sites always choose a regular octahedral coordination that includes V-O bond distances ranging from 1.90 to 2.18 Å.

The V^{IV} sites include a short V-O bond (from 1.56 to 1.72 Å). Among them, 73.5% choose a distorted octahedron with a short V-O bond, four intermediate bonds (from 1.82 to 2.10 Å) and a long bond (ranging from 2.10 to 2.70 Å) which is opposite to the short V-O bond. The other V^{IV} sites prefer three different five-fold coordinated environments (from square pyramid to trigonal bipyramid).

The V^{V} sites have several types of environments like octahedral, terahedral and pyramidal. Most of the $V^{V}O_x$ polyhedra include two short V-O bonds ranging from 1.84 to 2.06 Å. The longest distances (from 2.13 to 2.52 Å) exist in the $V^{V}O_6$ octahedra. This structure prefers two configurations: one of them includes two short V-O distances, two intermediate and two long bonds and the other configuration includes one short, four intermediate and one long V-O bond. The short bonds are opposite to the long bonds in these configurations. The $V^{V}O_5$ polyhedra involves two short and three intermediate bonds in a square pyramidal or in a half square pyramidal-half trigonal bipyramidal. The $V^{V}O_4$ tetrahedra usually prefer two short and two indermediate V-O distances (Boudin et al., 2000). Figure 3.2 shows some of the V-P-O polyhedral structures and vanadium phosphate compounds include cation. They are represented in light grey and middle grey, the PO_4 tetrahedra in dark grey and examples of AVPO structures in which cations are represented with dark grey circles.

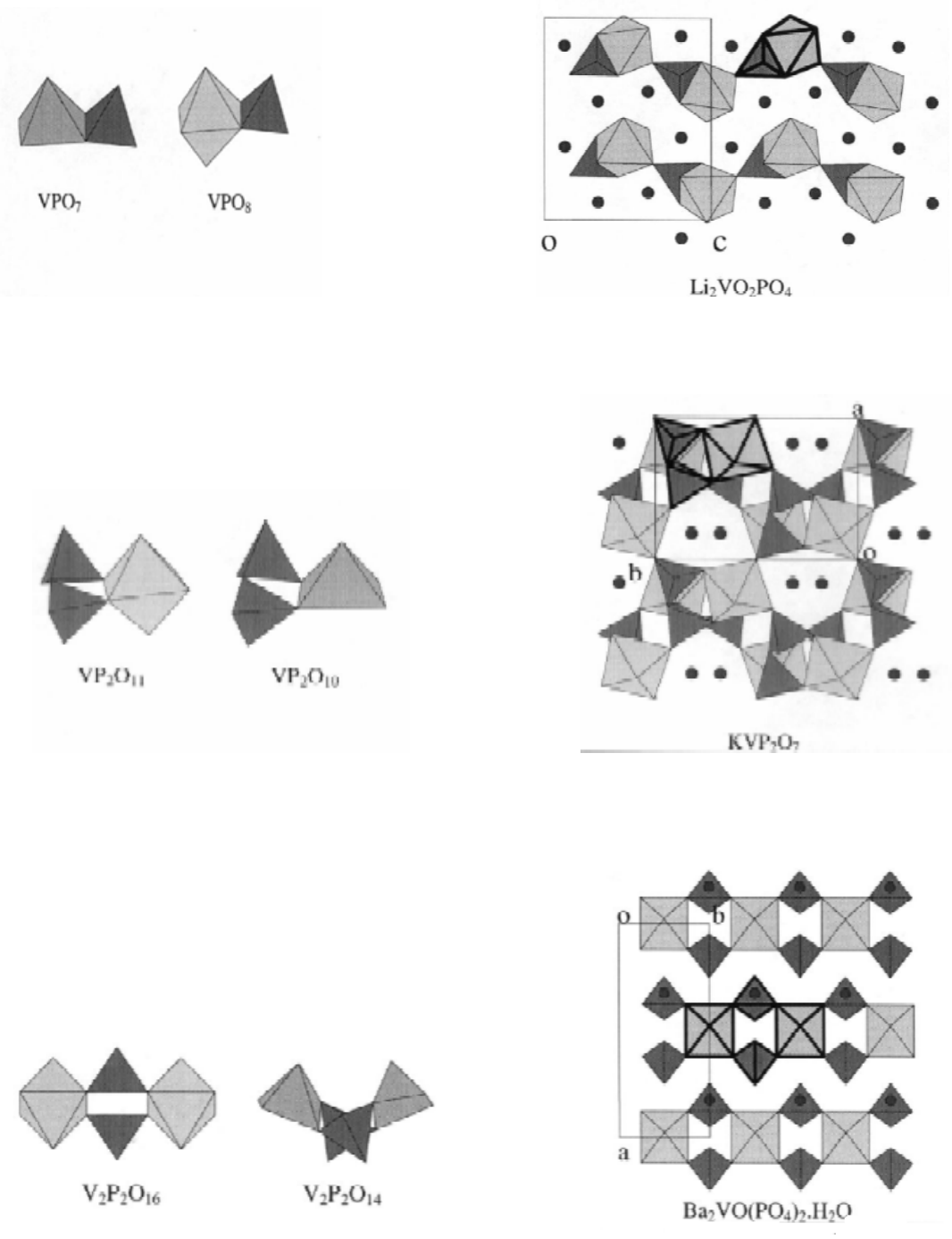

Figure 3.2. Most common mixed units composed of VO_5 and VO_6 polyhedra. (Source: Boudin et al., 2000)

3.2. Polyoxometalates

Polyoxometalates (POMs), as a large family of metal-oxygen clusters, have been predicted as ideal inorganic building blocks for the construction of large clusters or multidimensional enlarged organic-inorganic hybrid materials as they present a wide variety of stable structural motifs of different sizes and topologies. They are complex molecules whose structure has several metallic ions coordinated by shared oxide ions that form a highly symmetrical metal oxide.

3.2.1. History of Polyoxometalates

The history of the polyoxometalates started with the discovery of the first heteropoly salt, ammonium 12-molybdophosphate by Berzelius at 1826 and until 1908 nearly 750 heteropoly compounds had been reported. However, their structures had not been known until 1933. Keggin solved the most important type of heteropoly anions while he was studying $H_3[PW_{12}O_{40}].5H_2O$ molecule with powder X-ray diffraction in 1933. This structure, now named as Keggin structure, has 12 WO_6 octahedra linked by edge and corner sharing with the heteroatom occupying a tetrahedral hole in the center. The structure of another polyoxometalate, Anderson's heteropolyanion (6:1 series), was determined by Evans in 1948. Now, it is called as Anderson-Evans structure. After that, in 1953 a 18:2 heteropoly anion $[P_2W_{18}O_{62}]^{6-}$ was reported by Dawson and referred as Wells-Dawson's structure. Rather than these, in 1968 the structure of $[Ce^{4+}Mo_{12}O_{42}]^{8-}$ was reported by Dexter and Silverton. In this type of structure the large Ce heteroatom was in a CeO_{12} central icosahedron.

Today, the structures and properties of polyoxometalates are understood better by using modern characterisation techniques. Thus, many X-ray structures of them have already been reported. However, there are a lot of unanswered questions about their structures, mechanisms of synthesis, and reactivity (Kozhevnikov, 2002).

3.2.2. Structures of Polyoxometalates

Polyoxometalates are divided as isopolyanions or heteropolyanions due to the number of different types of atoms rather than oxygen. Isopolyanions have the formula $[M_mO_o]^{-p}$ and heteropolyanions which are illustrated in Figure 3.3, have the formula $[X_xM_mO_o]^{-q}$. M can be molybdenium, tungsten, vanadium, niobium and tantalum; X in heteropolyanions can be Si^V, P^{IV}, B^{III}, V^V (Gallegos, 2003).

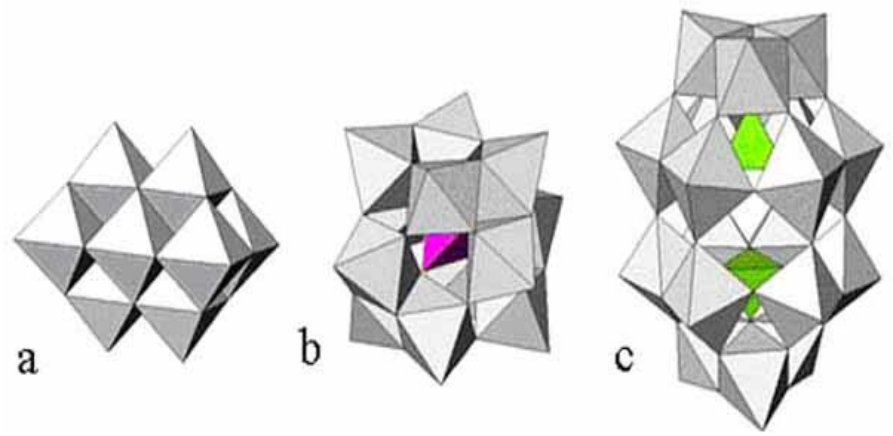

Figure 3.3. Polyhedral representations of isopolianions (a) decavanadate $(V_{10}O_{28})^{6-}$ and heteropolyanions (b) Keggin anion $(PMo_{12}O_{40})^{3-}$ (c) Wells-Dawson anion $(P_2W_{18}O_{62})^{6-}$. (Source: Casañ-Pastor and Gómez-Romero, 2004)

Heteropolyanions are the special types of polyoxometalate structures where XO_4 is the center of the molecule and surrounded by MO_6 octahedrons where M_3O_{13} is connected by sharing edges and to the XO_4 center by sharing corners. Keggin structure $[XM_{12}O_{40}]^{x-8}$ and the Wells-Dawson $[X_2M_{18}O_{62}]^{2x-16}$ structure are the most common and widely studied structures for this cluster type (Figure 3.4). Generally, the number of octahedrons in heteropolyanions changes from 12 to 48 and increase the sizes of them from a diameter of 10 Å (for Keggin structure) to 25 Å (for Wells-Dawson structure) (Gallegos, 2003).

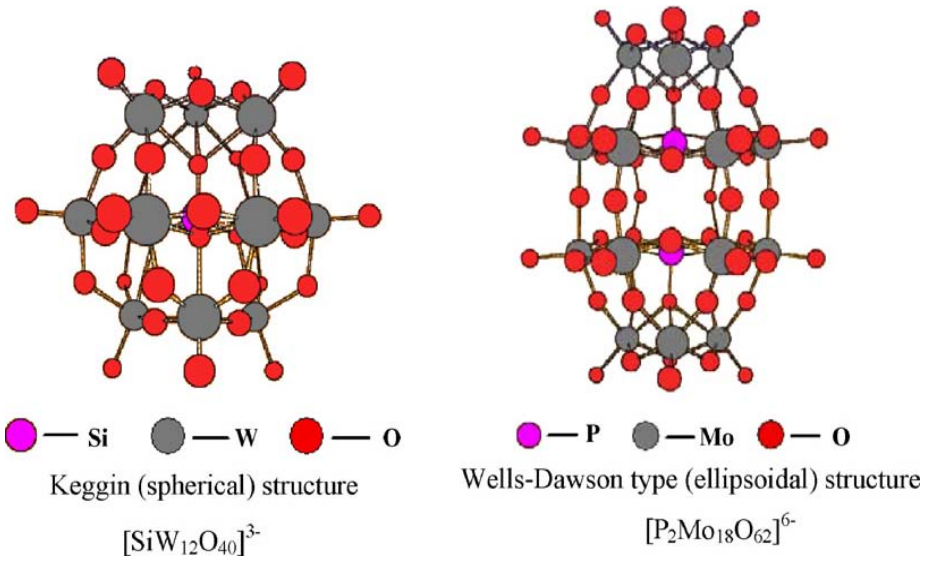

Figure 3.4. The structure of Keggin and Wells–Dawson type anion.
(Source: Li et al., 2007)

The Keggin structure is the most stable and easily available type of heteropoly compounds. In Keggin structure $[XM_{12}O_{40}]^{x-8}$, X is the heteroatom, x is the oxidation state and M is the addenda atom. Generally, M is Mo^{6+} or W^{6+}. The diameter of this structure is approximately 1.2 nm. In Wells-Dawson structure $[X_2M_{18}O_{62}]^{2x-16}$ generally X is P^{5+} or As^{5+} and M is Mo^{6+} or W^{6+}. Figure 3.5 and Figure 3.6 show the example structures of Keggin and Wells-Dawson type polyanions.

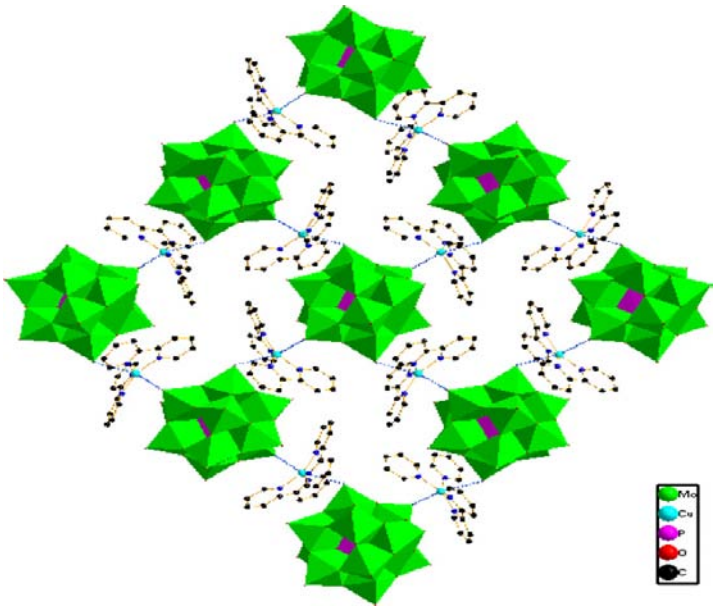

Figure 3.5. A grid network based on Keggin-type polyoxoanion, formulated [Cu(2,2'-bipy)$_2$](HPMo$_{12}$O$_{40}$).H$_2$O. (Source: Gao et al., 2007)

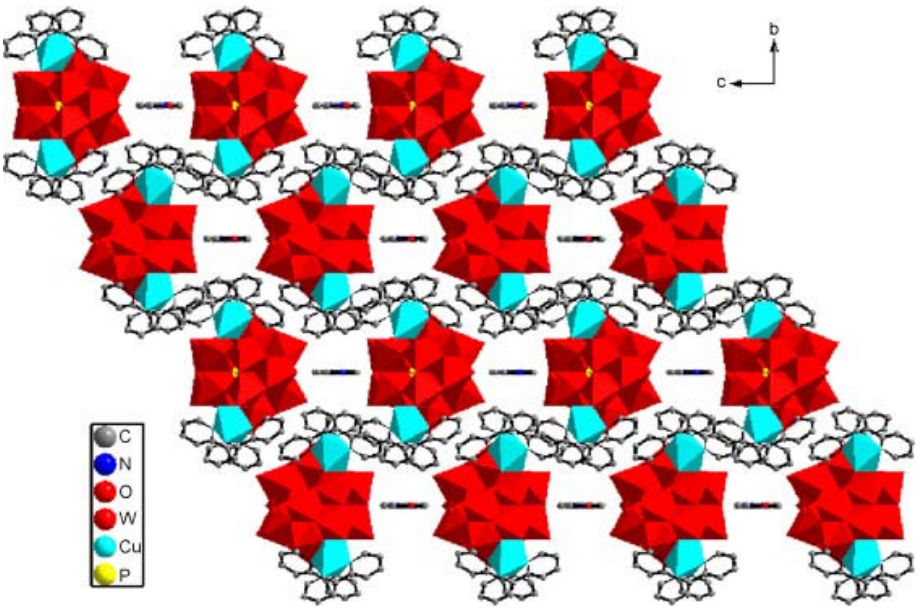

Figure 3.6. A grid network based on Wells-Dawson type polyoxoanion, formulated (dpdo)$_2$H$_2$[Cu(2,2'-bipy)$_2$]$_2$(P$_2$W$_{18}$O$_{62}$).5H$_2$O. (Source: Liu et al., 2009)

The Anderson-Evans structure is adopted by 6-heteropoly anions. This structure has six coplanar MO_6 octahedra arranged in a closed ring sharing edges. In the center of the ring, the heteroatom occupies an octahedral pocket.

The Dexter-Silverton structure is a less common type of 12-heteropolyanions $[XM_{12}O_{42}]^{x-12}$. Especially, M is Mo^{6+} and X is Ce^{4+}, U^{4+} or Th^{4+}. In this structure, twelve oxygen atoms surround the central atom to form an icosahedron and MO_6 octahedra are arranged in face-sharing pairs (Kozhevnikov, 2002).

Early transition metal oxide anion clusters (polyoxometalates or POMs) are quickly growing class of compounds and their sizes can affect the dimension of organic-inorganic hybrid POMs and copper is a good bridging body for multi-dimensional framefork assembly under hydrothermal conditions. The use of the well-defined metal oxide clusters for the construction of materials with more or less predictable connectivity in the crystalline state is attractive, since secondary metal-ligand bridges should provide linkages sufficiently strong to connect the clusters into kinetically stable crystal architectures.

$$M_xL_y(X_mO_n)_2 \longrightarrow \text{POMs formula} \qquad (3.1)$$

M_x : cationic metal center (template species)

L_y : polydentate organic ligand

$(X_mO_n)_2$: anionic polyoxometalate (building block) and (X_mO_n) also play the role of structure-directing effect for the constructions of such hybrid materials.

POMs have a coordination ability of polyoxoanion to combine with some transition metal coordination polymers and numerous 1D, 2D, 3D POM based hybrids have been synthesized successfully by Zubieta, Pope, Wang, Long, Niu and their coworkers. They have been interested by scientists because of their so-called ‘value adding properties’ and their conventional applications in photochemical response, conductivity, catalysis, medicine and studied as molecular models to resemble the chemical reactivity of solid metal oxide surface (Sha et al., 2007).

3.3. Synthesis and Characterization of Compounds

3.3.1. Synthesis and Characterization of $NaCo_3(PO_4)(HPO_4)_2$

$NaCo_3(PO_4)(HPO_4)_2$ pink crystals were synthesized by hydrothermal reaction of $Na_2WO_4.2H_2O$ (0.3287 g), $Co(NO_3)_2.6H_2O$ (0.2945 g), 4,4'-bipyridine (0.1020 g), 5M H_3PO_4 (0.5 ml) and H_2O (7.0 ml) at 170˚C for 3 days in a 23 ml Teflon-lined autoclave. $Na_2WO_4.2H_2O$ (Sigma-Aldrich, 99%), $Co(NO_3)_2.6H_2O$ (Merck, 99%), 4,4'-bipyridine (Alfa Aesar, 98%), 5M H_3PO_4 (Sigma-Aldrich, 85%) were used without purification.

After all reactants were loaded into the vessel, the mixture was stirred for 20 minutes at laboratory conditions. At the end of stirring, teflon vessel was put into the steel autoclave and heated at 170˚C for 3 days in oven. When the reaction finished, the autoclave was slowly cooled at room temperature. The product was filtered by vacuum filtration and washed several times with pure water. The pink crystals were obtained on filter paper by optical microscope. Crystals were characterized by SEM-EDX and single crystal X-ray diffraction methods.

$$\underset{0.3287g}{Na_2WO_4.2H_2O} + \underset{0.2945g}{Co(NO_3)_2.6H_2O} + \underset{0.1020g}{4,4'\text{-bpy}} + \underset{0.5\ ml}{H_3PO_4} + \underset{7\ ml}{H_2O} \qquad (3.2)$$

$$\xrightarrow[3\ days]{170\ ^\circ C}$$

pink crystals

According to the SEM/EDX results of the pink crystals shown in Figure 3.7, the compound contains Na, O, P, Co elements in the weight percentages 3.52%, 43.11%, 17.37% and 30.96% respectively.

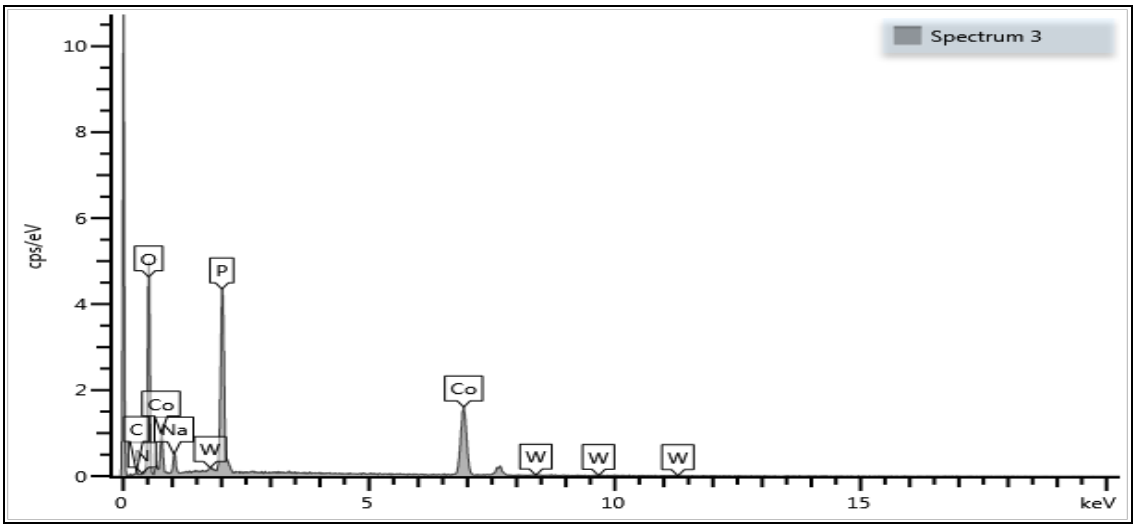

Figure 3.7. SEM/EDX spectrum of $NaCo_3(PO_4)(HPO_4)_2$.

3.3.1.1. X-ray Crystallographic Analysis of $NaCo_3(PO_4)(HPO_4)_2$

Single crystal X-ray diffraction of the resulting crystals was performed using a Rigaku AFC8S diffractometer equipped with Mo Kα (λ=0.71073 Å) radiation and a Mercury CCD area detector. Data collection and processing including corrections for absorption and Lorentz and polarization effects were performed using the CrystalClear software package (Version 1.3. Rigaku Corporation, Japan and MSC, The Woodlands, Texas, USA). Candidate space groups were identified based on the systematic absences of the data. The structures were solved by direct methods and refined by full-matrix least squares on F^2 using the SHELXTL software package. All atoms were refined anisotropically in the structures.

Crystallographic data are given in Table 3.1. Selected bond lengths (Å) and bond angles (degree) for $NaCo_3(PO_4)(HPO_4)_2$ are given in Table 3.2 and Table 3.3 respectively.

Table 3.1. Crystallographic data for $NaCo_3(PO_4)(HPO_4)_2$.

	(**1**)
Empirical Formula	$NaCo_3H_2P_3O_{12}$
Formula weight	486.69
Space group	C2/c
a, Å	11.872(2)
b, Å	12.150(2)
c, Å	6.5107(13)
α, °	90.00
β, °	114.07(3)
γ, °	90.00
V, $Å^3$	857.5(3)
Z	4
D_{calc}, Mg/m^3	3.754
Parameters	88
μ, mm^{-1}	6.421
θ range, °	2.5181-26.70
Reflections	
Collected	4104
Independent	910
Observed [I≥2σ(I)]	703
R (int)	0.0605
Final R (obs. data)[a]	
R_1	0.0469
wR_2	0.1112
Final R (all data)	
R_1	0.0644
wR_2	0.1224
Goodness of fit on F^2	1.071
Largest diff. peak, $e/Å^3$	1.324
Largest diff. hole, $e/Å^3$	-1.421

Table 3.2. Selected bond lengths (Å) for $NaCo_3(PO_4)(HPO_4)_2$.

Co(1) – O(1)	2.130(4)	Co(2) – O(1)	2.127(5)
Co(1) – O(1)	2.130(4)	Co(2) – Na(1)	3.161(4)
Co(1) – O(2)	2.140(5)	P(1) – O(6)	1.538(5)
Co(1) – O(2)	2.140(5)	P(1) – O(6)	1.538(5)
Co(1) – O(3)	2.185(5)	P(1) – O(1)	1.555(4)
Co(1) – O(3)	2.185(5)	P(1) – O(1)	1.555(4)
Co(2) – O(5)	2.055(5)	P(2) – O(4)	1.517(5)
Co(2) – O(2)	2.080(5)	P(2) – O(5)	1.526(5)
Co(2) – O(4)	2.093(5)	P(2) – O(2)	1.530(5)
Co(2) – O(6)	2.100(5)	P(2) – O(3)	1.590(5)
Co(2) – O(4)	2.106(4)		

Table 3.3. Selected bond angles (°) for $NaCo_3(PO_4)(HPO_4)_2$.

O(1) – Co(1) – O(1)	155.4(2)	O(1) – Co(2) – Na(1)	64.84(16)
O(1) – Co(1) – O(2)	86.84(17)	P(2) – O(2) – Co(1)	134.4(3)
O(1) – Co(1) – O(2)	77.94(18)	Co(2) – O(2) – Co(1)	100.97(19)
O(2) – Co(1) – O(2)	103.5(3)	O(6) – P(1) – O(6)	107.0(4)
O(1) – Co(1) – O(3)	89.55(17)	O(6) – P(1) – O(1)	109.0(2)
O(2) – Co(1) – O(3)	83.88(18)	O(1) – P(1) – O(1)	109.9(4)
O(1) – Co(1) – O(3)	89.55(17)	O(4) – P(2) – O(5)	110.6(3)
O(3) – Co(1) – O(3)	89.3(2)	O(5) – P(2) – O(2)	109.4(3)
O(5) – Co(2) – O(2)	85.49(18)	O(2) – P(2) – O(3)	108.4(3)
O(2) – Co(2) – O(4)	90.75(17)	O(4) – P(2) – Na(1)	127.8(2)
O(4) – Co(2) – O(6)	85.38(18)	O(5) – P(2) – Na(1)	43.4(2)
O(6) – Co(2) – O(4)	85.37(19)	O(3) – P(2) – Na(1)	122.27(19)
O(5) – Co(2) – Na(1)	46.61(17)	Na(1) – P(2) – Na(1)	61.99(5)
O(2) – Co(2) – Na(1)	104.73(14)	P(1) – O(1) – Co(2)	124.1(3)
O(4) – Co(2) – Na(1)	142.60(17)	P(1) – O(1) – Co(1)	125.4(3)
O(6) – Co(2) – Na(1)	118.39(15)	Co(2) – O(1) – Co(1)	99.76(19)

3.3.1.2. Results and Discussion for $NaCo_3(PO_4)(HPO_4)_2$

The compound $NaCo_3(PO_4)(HPO_4)_2$ was synthesized by hydrothermal method as pink crystals from the reaction of $Na_2WO_4.2H_2O$, $Co(NO_3)_2.6H_2O$, 4,4'-bipyridine and HPO_4.

As a result of single crystal X-ray diffraction analysis, it is determined that CoO_6 octahedra in the structure form chains by corner sharing which are illustrated in Figure 3.8.

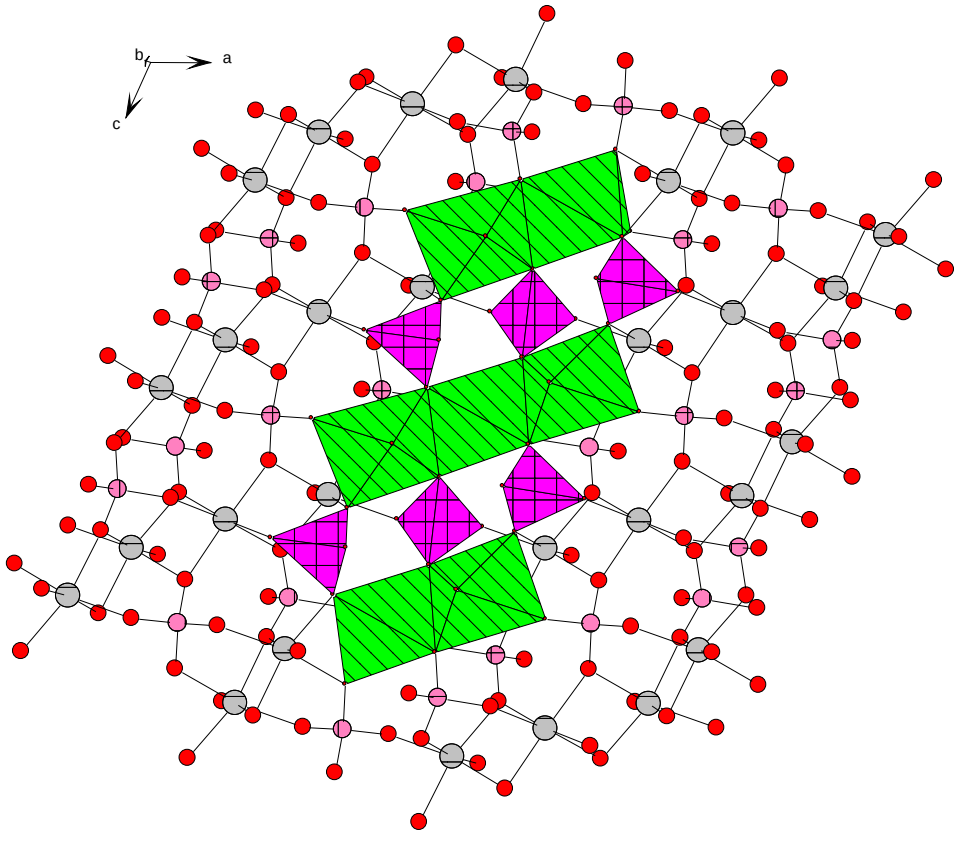

Figure 3.8. The view of $NaCo_3(PO_4)(HPO_4)_2$ crystal that includes the polyhedral structures.

These chain structures connect to the PO_4 and HPO_4 groups and build up adjacent layers. Moreover, these adjacent layers construct two different channels through the c-axis. One of these channels is along the [1/2, 0, z] direction, whether the other channel is along the [0, 0, z] direction and does not consist of any Na atoms.

Asymmetric unit involves Na, Co(1) and P(1) atoms on two-fold axis and Co(2), P(2) and six O atoms in general position which were shown in Figure 3.9.

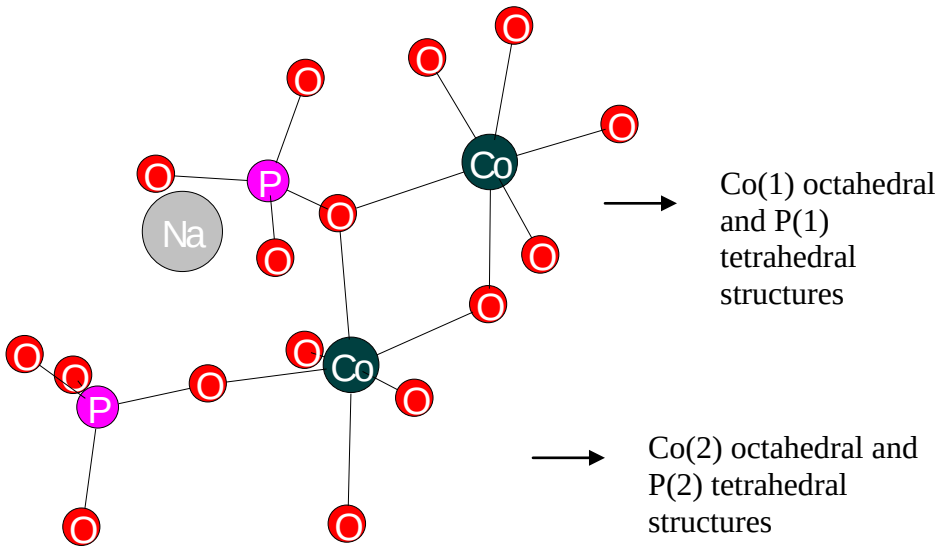

Figure 3.9. The unit structure view of $NaCo_3(PO_4)(HPO_4)_2$.

Co(1) atom appears on two-fold axis. While each $Co(1)O_6$ octahedra is sharing the edges with $Co(2)O_6$, each $Co(2)O_6$ shares the edges with $Co(1)O_6$ and $Co(2)O_6$. O atoms in these sharing edges make bonds with $P(1)O_4$ and $HP(2)O_4$ groups at the same time. The octahedral structures which form the chain, are connected by two O atoms of PO_4 group. The other oxygens in PO_4 attach the CoO_6 chains. Na atoms fill the spaces in the structure and fall into the corners and middle of the unit cell.

While the two oxygens of HPO_4 group are linking the octahedra in the chain, one of the remaining oxygens connects the chains in the same layer and the other one provides the linkage between the layers which are illustrated in Figure 3.10.

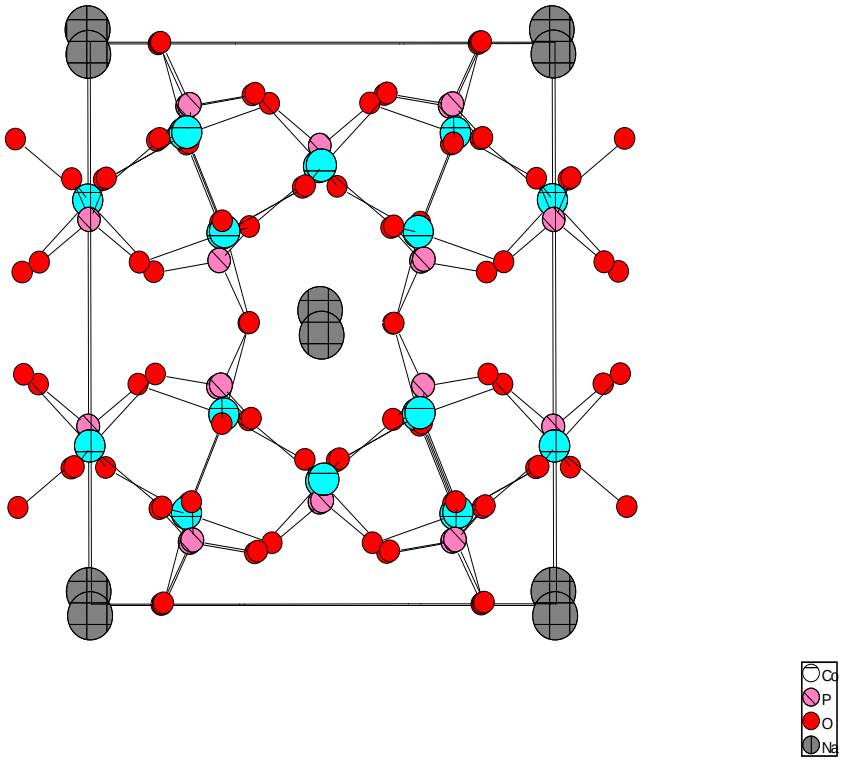

Figure 3.10. The unitcell view of $NaCo_3(PO_4)(HPO_4)_2$.

The bond distances of Co(1) atom with the oxgens are between 2.130(4) and 2.185(5) Å, whereas the bond distances of of Co(2) atom with the oxgens are between 2.055(5) and 2.127(5) Å. Therefore, the distances of P(1)-O bonds are between 1.538(5) and 1.555(4) Å, the distances of P(2)-O bonds are between 1.517(5) and 1.590(5) Å. Lastly, the interactions of Na atom with oxygens fall in ranges of 2.300(5)-2.966(7) Å.

The bond valence sums of $NaCo_3(PO_4)(HPO_4)_2$ shown in Table 3.4 were calculated by Bond Valence Sum, BVS method developed by ID Brown. Although the charge of Co(1) atom is lower than the other Co atoms, generally, it is in accord with the formal oxidation states. The charge of each Co atom is 2+. Also, it is observed that, the bond valence sums of O(3) and O(6) are 1.34 and 1.57 respectively and this shows the H atoms which are attached to these oxygens for providing the charge balance. Moreover, the bond between the O(3) and O(6) atoms in different PO_4 groups whose distance is 2.485 Å, shows the H bonds. Finally, the charge of each oxygen atom rather

than O(3) and O(6) is found as 2- and the charges of P and Na atoms are found in order of 5+ and 1+ from the calculations.

Table 3.4. Bond valence sums of $NaCo_3(PO_4)(HPO_4)_2$.

	Na(1)	P(1)	P(2)	Co(1)	Co(2)	∑
O(1)	0.043	1.182		0.612	0.309	2.146
O(2)	0.104		1.265	0.596	0.350	1.965
O(3)			1.076	0.528		1.340
O(4)			1.310		0.665	1.975
O(5)	0.623		1.279		0.375	2.096
O(6)		1.238			0.332	1.570
P(2)	0.220					
Na(1)			0.220			
∑	0.990	4.840	5.150	1.736	2.031	

3.3.2. Synthesis and Characterization of $Co(4,4'\text{-bpy})_2(VO_2)_2(HPO_4)_2$

$Co(4,4'\text{-bpy})_2(VO_2)_2(HPO_4)_2$ red crystals were synthesized with hydrothermal reaction of $Na_2WO_4.2H_2O$ (0.3233 g), $NaVO_3$(0.1200 g), $Co(NO_3)_2.6H_2O$ (0.2942 g), 4,4'-bipyridine (0.1026 g), 5M H_3PO_4 (0.3 ml) and H_2O (7.0 ml) at 170˚C for 3 days in a 23 ml Teflon-lined autoclave. $Na_2WO_4.2H_2O$ (Sigma-Aldrich, 99%), $Co(NO_3)_2.6H_2O$ (Merck, 99%), $NaVO_3$ (Sigma-Aldrich, 98%), 4,4'-bipyridine (Alfa Aesar, 98%), 5M H_3PO_4 (Sigma-Aldrich, 85%) were used without purification.

After all reactants were loaded into the vessel, the mixture was stirred for 20 minutes at laboratory conditions. At the end of stirring, teflon vessel was put into the steel autoclave and heated at 170˚C for 3 days in oven. When the reaction finished, the autoclave was slowly cooled at room temperature. The product was filtered by vacuum filtration and washed several times with pure water. The red crystals were obtained on filter paper by optical microscope. Crystals were characterized by SEM-EDX and single crystal X-ray diffraction methods.

$$Na_2WO_4.2H_2O + NaVO_3 + Co(NO_3)_2.6H_2O + 4,4'\text{-bpy} + H_3PO_4 + H_2O \quad (3.3)$$
0.3233g 0.1200g 0.2942g 0.1026g 0.3 ml 7 ml

170 ° C | 3 days

red crystals

According to the SEM/EDX results of the red crystals shown in Figure 3.11, the compound contains C, N, O, V, P and Co elements in the weight percentages 18.05%, 4.35%, 68.19%, 3.90%, 3.06% and 1.92% respectively.

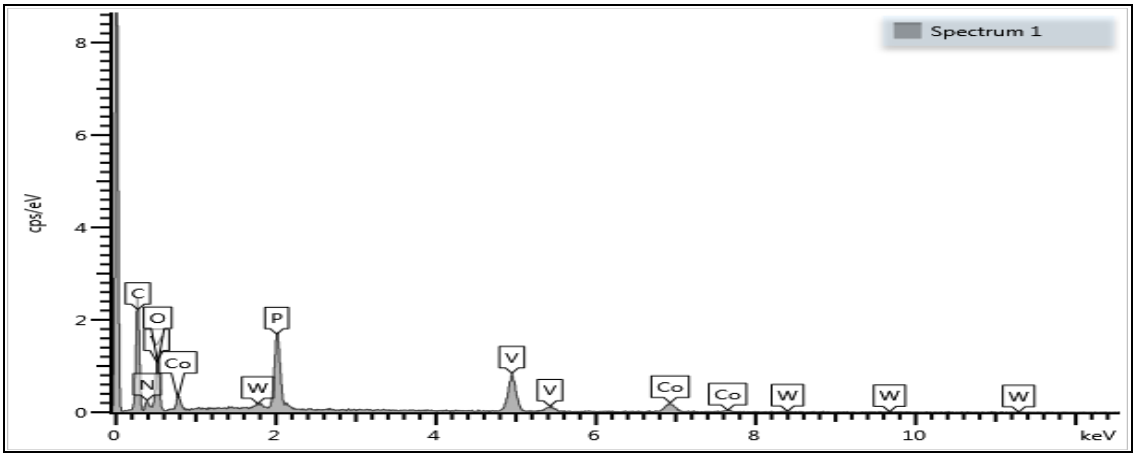

Figure 3.11. SEM/EDX spectrum of $Co(4,4'\text{-bpy})_2(VO_2)_2(HPO_4)_2$.

3.3.2.1. X-ray Crystallographic Analysis of $Co(4,4'\text{-bpy})_2(VO_2)_2(HPO_4)_2$

Single crystal X-ray diffraction of the resulting crystals was performed using a Rigaku AFC8S diffractometer equipped with Mo Kα (λ=0.71073 Å) radiation and a Mercury CCD area detector. Data collection and processing including corrections for absorption and Lorentz and polarization effects were performed using the CrystalClear software package (Version 1.3. Rigaku Corporation, Japan and MSC, The Woodlands, Texas, USA). Candidate space groups were identified based on the systematic absences of the data. The structures were solved by direct methods and refined by full-matrix

least squares on F^2 using the SHELXTL software package. All atoms were refined anisotropically in the structures.

Crystallographic data are given in Table 3.5. Selected bond lengths (Å) and bond angles (degree) for $Co(4,4'\text{-bpy})_2(VO_2)_2(HPO_4)_2$ are given in Table 3.6 and Table 3.7 respectively.

Table 3.5. Crystallographic data for $Co(4,4'\text{-bpy})_2(VO_2)_2(HPO_4)_2$.

	(**1**)
Empirical Formula	$C_{20}H_{18}N_4O_{12}P_2V_2$
Formula weight	715.53
Space group	C2/c
a, Å	25.1790(5)
b, Å	8.1257(16)
c, Å	15.6403(3)
α, °	90.00
β, °	127.32(3)
γ, °	90.00
V, $Å^3$	2544.9(9)
Z	4
D_{calc}, Mg/m^3	1.903
Parameters	187
μ, mm^{-1}	1.562
θ range, °	2.71-26.35
Reflections	
Collected	11498
Independent	2578
Observed [I≥2σ(I)]	2331
R (int)	0.0192
Final R (obs. data)[a]	
R_1	0.0348
wR_2	0.0898
Final R (all data)	
R_1	0.0392
wR_2	0.0955
Goodness of fit on F^2	0.946
Largest diff. peak, e/$Å^3$	0.667
Largest diff. hole, e/$Å^3$	0.649

Table 3.6. Selected bond lengths (Å) for Co(4,4'-bpy)$_2$(VO$_2$)$_2$(HPO$_4$)$_2$.

Co(1) – O(1)	2.053(2)	N(1) – C(9)	1.322(5)
Co(1) – O(1)	2.053(2)	N(1) – C(7)	1.329(4)
Co(1) – O(2)	2.098(2)	N(2) – C(3)	1.329(4)
Co(1) – O(2)	2.098(2)	N(2) – C(4)	1.329(5)
Co(1) – N(2)	2.126(3)	C(1) – C(2)	1.383(4)
Co(1) – N(2)	2.126(3)	C(1) – C(5)	1.390(5)
V(1) – O(6)	1.616(2)	C(1) – C(6)	1.481(4)
V(1) – O(2)	1.632(2)	C(2) – C(3)	1.383(5)
V(1) – O(3)	1.949(2)	C(4) – C(5)	1.379(5)
V(1) – O(4)	1.989(2)	C(6) – C(8)	1.374(5)
V(1) – N(1)	2.165(3)	C(6) – C(10)	1.385(5)
P(1) – O(1)	1.502(2)	C(7) – C(10)	1.384(5)
P(1) – O(3)	1.537(2)	C(8) – C(6)	1.374(5)
P(1) – O(4)	1.549(2)	C(8) – C(9)	1.386(5)
P(1) – O(5)	1.576(2)	C(10) – C(6)	1.385(5)

Table 3.7. Selected bond angles (°) for Co(4,4'-bpy)$_2$(VO$_2$)$_2$(HPO$_4$)$_2$.

O(1) – Co(1) – O(1)	180.00(9)	O(2) – Co(1) – N(2)	87.13(11)
O(1) – Co(1) – O(2)	88.27(9)	N(2) – Co(1) – N(2)	180.00(14)
O(1) – Co(1) – O(2)	91.73(9)	O(6) – V(1) – O(2)	109.71(14)
O(1) – Co(1) – O(2)	91.73(9)	O(6) – V(1) – O(3)	128.58(12)
O(1) – Co(1) – O(2)	88.27(9)	O(2) – V(1) – O(3)	120.79(11)
O(2) – Co(1) – O(2)	180.0(3)	O(6) – V(1) – O(4)	98.03(11)
O(1) – Co(1) – N(2)	89.45(9)	O(2) – V(1) – O(4)	96.43(11)
O(1) – Co(1) – N(2)	90.55(9)	O(3) – V(1) – O(4)	85.98(9)
O(2) – Co(1) – N(2)	87.13(11)	O(6) – V(1) – N(1)	88.75(11)
O(2) – Co(1) – N(2)	92.87(11)	O(2) – V(1) – N(1)	91.20(11)
O(1) – Co(1) – N(2)	90.55(9)	O(3) – V(1) – N(1)	81.50(9)
O(1) – Co(1) – N(2)	89.45(9)	O(4) – V(1) – N(1)	167.40(9)
O(2) – Co(1) – N(2)	92.87(11)	O(1) – P(1) – O(3)	111.77(12)
O(1) – P(1) – O(4)	111.95(12)	O(3) – P(1) – O(8)	106.67(12)
O(3) – P(1) – O(4)	108.59(12)	O(4) – P(1) – O(8)	108.33(13)
O(1) – P(1) – O(8)	109.33(12)		

3.3.2.2. Results and Discussion for $Co(4,4'\text{-bpy})_2(VO_2)_2(HPO_4)_2$

The compound $Co(4,4'\text{-bpy})_2(VO_2)_2(HPO_4)_2$ was synthesized by hydrothermal method as red crystals from the reaction of $Na_2WO_4.2H_2O$, $NaVO_3$, $Co(NO_3)_2.6H_2O$, 4,4'-bipyridine and HPO_4.

The result of single crystal X-ray diffraction analysis shows that the three dimensional crystal structure whose unitcell view is shown in Figure 3.12 consists of $[(VO_2)(HPO_4)]_\infty$ helical chains and $[Co(4,4'\text{-bpy})_2]^{2+}$ frameworks.

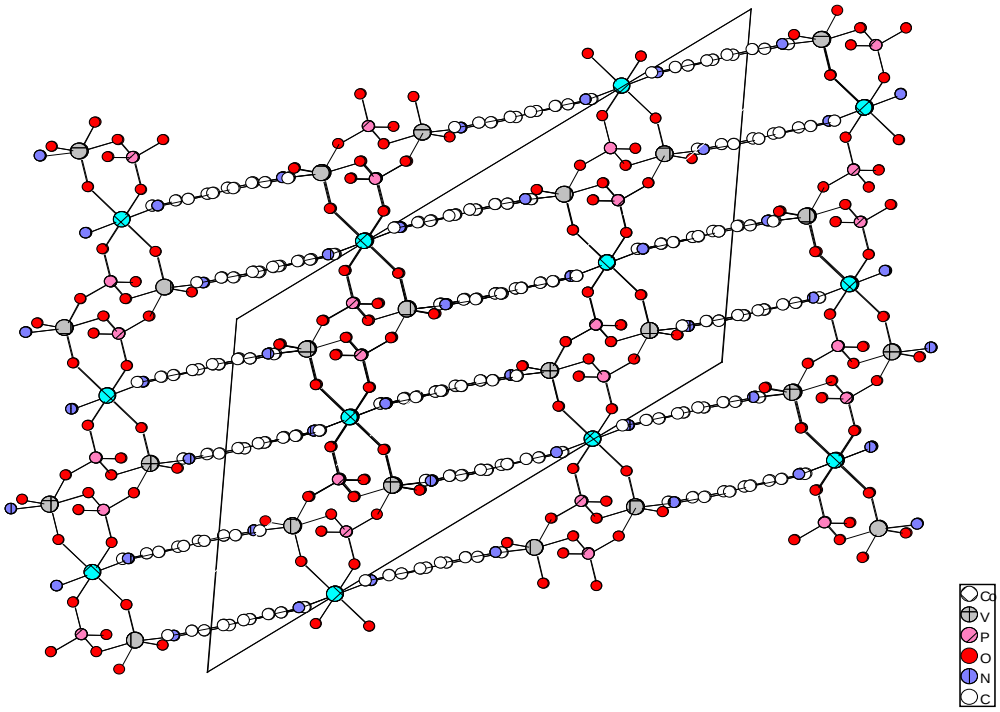

Figure 3.12. The unitcell view of $Co(4,4'\text{-bpy})_2(VO_2)_2(HPO_4)_2$.

The chains are constructed by the alternate connection of HPO_4 tetrahedra and VO_4N trigonal bipyramids by sharing the edges and these helical $[(VO_2)(HPO_4)]_\infty$ chains connect to the CoO_4N_2 octahedra and form the $[CoV_2P_2O_{12}]$ layer pattern which are illustrated in Figure 3.13 and Figure 3.14.

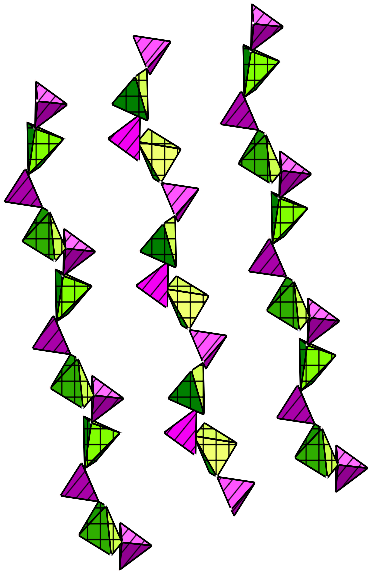

Figure 3.13. The view of the helical structure that consists of HPO_4 tetrahedra and VO_4N trigonal bipyramids.

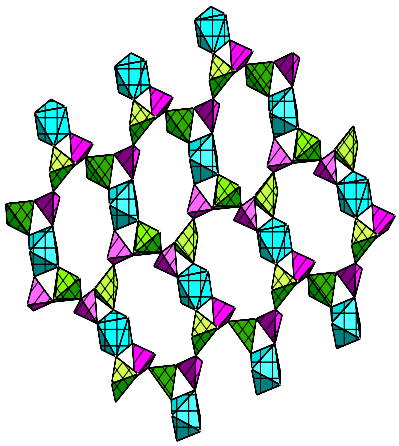

Figure 3.14. Polyhedral view of $Co(4,4'\text{-bpy})_2(VO_2)_2(HPO_4)_2$.

The 3-dimensional structure is composed of the bonds of these layers with 4,4'-bipyridine ligands that is shown in Figure 3.15 and in the crystal, vanadium trigonal bipyramids constitute distorted trigonal bipyramidal structures by connecting with four oxygen atoms and a nitrogen atom of 4,4'-bipyridine ligand. The three oxygen atoms are located in the equatorial position and the remaining oxygen is the terminal atom. The three oxygen atoms in equatorial position act as bridging atoms between vanadium and phosphorus, vanadium and cobalt alternately.

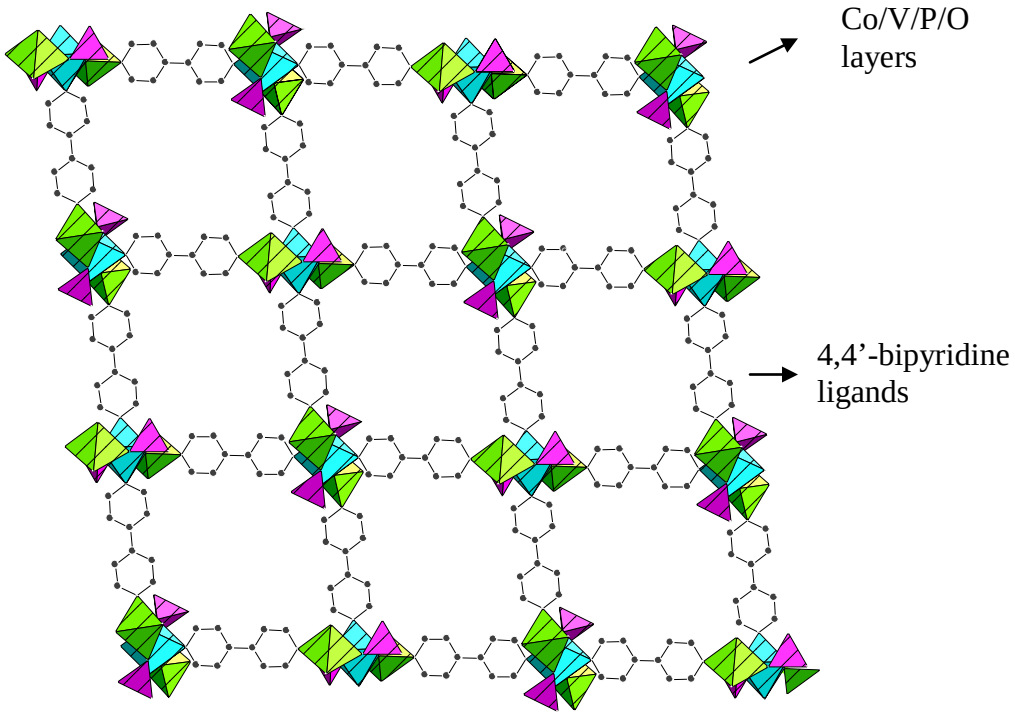

Figure 3.15. The view of $Co(4,4'\text{-bpy})_2(VO_2)_2(HPO_4)_2$ structure that includes Co/V/P/O layers and 4,4'-bipyridine ligands.

The two oxygens of PO_4 tetrahedra connect to the vanadium atoms (V-O-P) and remaining oxgens of this tetrahedra link to a cobalt atom (Co-O-P) and a H atom (P-O-H). Co atom in octahedral structure makes two bonds with VO_4N group, two bonds with HPO_4 group in equatorial position and also, it is linked to two 4,4'-bipyridine ligands from their N atoms which are shown in Figure 3.16.

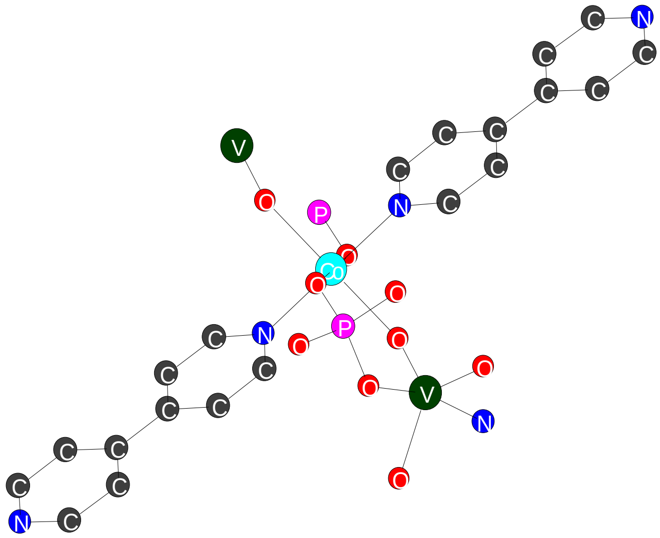

Figure 3.16. The coordination of Co atom in $Co(4,4'\text{-bpy})_2(VO_2)_2(HPO_4)_2$.

In $Co(4,4'\text{-bpy})_2(VO_2)_2(HPO_4)_2$ crystal, Co atom connects to four oxygen and two nitrogen atoms totally. The Co-O bond distances are 2.053(2) and 2.098(2) Å, each Co-N bond distance is 2.126(3) Å. V atom connects to four oxygen atoms and one nitrogen atom totally. The distances of V-O bonds are between 1.616(2) and 1.989(2) Å. The distance of each V-N bond is 2.165(3) Å. Finally, the distances of P-O bonds in PO_4 tetrahedra fall in the ranges of 1.502(2)-1.576(2) Å and all bonds in the structure are single bonds.

The bond valence sums of $Co(4,4'\text{-bpy})_2(VO_2)_2(HPO_4)_2$ shown in Table 3.8 were calculated by Bond Valence Sum, BVS method developed by ID Brown. The results of these calculations show that the oxidation states of V, P, Co and O atoms of the structure are 5+, 5+, 2+ and 2- respectively. Only the valence sum of O(5) atom was calculated as 1.12 and this shows the existence of the H atom connected to this O atom that provides the charge balance.

Table 3.8. Bond valence sums of $Co(4,4'\text{-bpy})_2(VO_2)_2(HPO_4)_2$.

	V(1)	P(1)	Co(1)	∑
O(1)		1.365	0.754	2.119
O(2)	1.588		0.668	2.256
O(3)	0.674	1.241		1.915
O(4)	0.605	1.202		1.807
O(5)		1.117		1.117
O(6)	1.658			1.658
N(1)	0.475			0.475
N(2)			0.806	0.806
∑	5.000	4.925	2.228	

3.3.3. Synthesis and Characterization of $(enH_2)_3[Co_3W_4P_4O_{28}]$

$(enH_2)_3[Co_3W_4P_4O_{28}]$ dark blue crystals were synthesized by hydrothermal reaction of $Na_2WO_4.2H_2O$ (0.3266 g), $Co(NO_3)_2.6H_2O$ (0.2995 g), 5M ethylenediamine (0.5 ml), 5M H_3PO_4 (0.2 ml) and H_2O (7.0 ml) at 170˚C for 3 days in a 23 ml Teflon-lined autoclave. $Na_2WO_4.2H_2O$ (Sigma-Aldrich, 99%), $Co(NO_3)_2.6H_2O$ (Merck, 99%), ethylenediamine (Merck, 99%), H_3PO_4 (Sigma-Aldrich, 85%) were used without further purification.

After all reactants were loaded into the vessel, the mixture was stirred for 20 minutes at laboratory conditions. At the end of stirring, teflon vessel was put into the steel autoclave and heated at 170˚C for 3 days in oven. When the reaction finished, the autoclave was slowly cooled at room temperature. The product was filtered by vacuum filtration and washed several times with pure water. The dark blue crystals were obtained on filter paper by optical microscope. Crystals were characterized by powder X-ray diffraction, SEM-EDX, single crystal X-ray diffraction methods.

$$Na_2WO_4.2H_2O + Co(NO_3)_2.6H_2O + \text{etylenediamine} + H_3PO_4 + H_2O \quad (3.4)$$
0.3266g 0.2995g 0.5 ml 0.2 ml 7 ml

170 ° C, 3 days ↓

blue crystals

According to the SEM/EDX results of the dark blue crystals shown in Figure 3.17, the compound contains C, N, O, W, P and Co elements in the weight percentages 25.17%, 8.57%, 29.45%, 30.89%, 4.28% and 1.03% respectively.

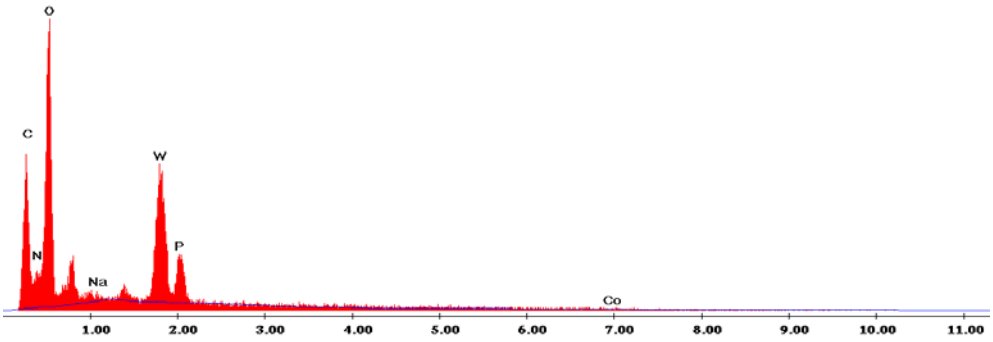

Figure 3.17. SEM/EDX spectrum of $(enH_2)_3[Co_3W_4P_4O_{28}]$.

The synthesized compound was analyzed by powder X-ray diffractometer. The powder peaks of the compound which are shown in Figure 3.18 did not match well with any of the compounds in the XRD database.

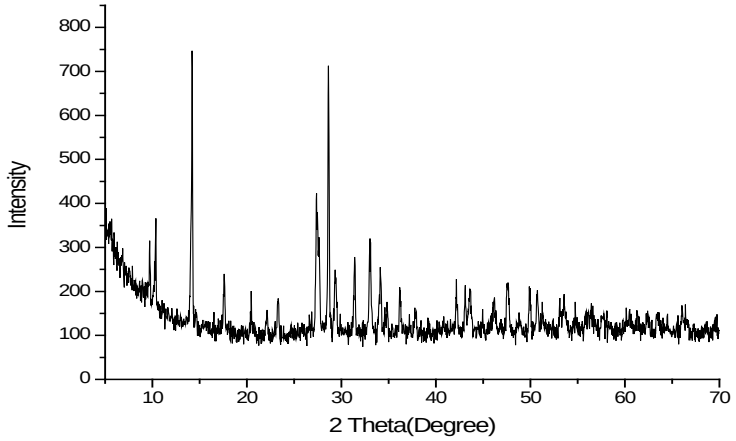

Figure 3.18. XRD spectrum of $(enH_2)_3[Co_3W_4P_4O_{28}]$.

3.3.3.1. X-ray Crystallographic Analysis of $(enH_2)_3[Co_3W_4P_4O_{28}]$

Single crystal X-ray diffraction of the resulting crystals was performed using a Rigaku AFC8S diffractometer equipped with Mo Kα (λ=0.71073 Å) radiation and a Mercury CCD area detector. Data collection and processing including corrections for absorption and Lorentz and polarization effects were performed using the CrystalClear software package (Version 1.3. Rigaku Corporation, Japan and MSC, The Woodlands, Texas, USA). Candidate space groups were identified based on the systematic absences of the data. The structures were solved by direct methods and refined by full-matrix least squares on F^2 using the SHELXTL software package. All atoms were refined anisotropically in the structures.

Crystallographic data are given in Table 3.9. Selected bond lengths (Å) and bond angles (degree) for $(enH_2)_3[Co_3W_4P_4O_{28}]$ are given in Table 3.10. and Table 3.11. respectively.

Table 3.9. Crystallographic data for $(enH_2)_3[Co_3W_4P_4O_{28}]$.

	(**1**)
Empirical Formula	$Co_3W_4P_4O_{28}C_6N_6H_{30}$
Formula weight	1666.11
Space group	I4(1)/a
a, Å	17.138(2)
b, Å	17.138(2)
c, Å	10.775(2)
α, °	90.00
β, °	90.00
γ, °	90.00
V, $Å^3$	3164.6(9)
Z	4
D_{calc}, Mg/m^3	3.224
Parameters	141
μ, mm^{-1}	4.182
θ range, °	2.2327-26.59
Reflections	
Collected	14693
Independent	1662
Observed [I≥2σ(I)]	1476
R (int)	0.0569
Final R (obs. data)[a]	
R_1	0.0416
wR_2	0.1072
Final R (all data)	
R_1	0.0479
wR_2	0.1127
Goodness of fit on F^2	1.123
Largest diff. peak, $e/Å^3$	2.682
Largest diff. hole, $e/Å^3$	-1.841

Table 3.10. Selected bond lengths (Å) for $(enH_2)_3[Co_3W_4P_4O_{28}]$.

W(1) – O(6)	1.774(9)	Co(3) – O(3)	1.936(9)
W(1) – O(4)	1.774(9)	Co(3) – O(3)	1.936(9)
W(1) – O(5)	1.831(9)	Co(3) – O(3)	1.936(9)
W(1) – O(1)	2.077(9)	Co(3) – O(3)	1.936(9)
W(1) – O(7)	2.127(9)	P(5) – O(2)	1.522(10)
W(1) – O(5)	2.139(9)	P(5) – O(3)	1.522(10)
Co(2) – O(4)	2.082(9)	P(5) – O(1)	1.545(9)
Co(2) – O(4)	2.082(9)	P(5) – O(7)	1.548(9)
Co(2) – O(6)	2.104(10)	C(1) – N(1)	1.500(3)
Co(2) – O(6)	2.104(10)	C(1) – N(1)	1.500(3)
Co(2) – O(2)	2.113(9)	C(1) – C(1)	1.500(6)
Co(2) – O(2)	2.113(9)		

Table 3.11. Selected bond angles (°) for $(enH_2)_3[Co_3W_4P_4O_{28}]$.

O(6) – W(1) – O(4)	100.8(4)	O(4) – Co(2) – O(2)	91.0(4)
O(6) – W(1) – O(5)	98.1(4)	O(6) – Co(2) – O(2)	89.1(4)
O(4) – W(1) – O(5)	98.4(4)	O(6) – Co(2) – O(2)	90.9(4)
O(6) – W(1) – O(1)	89.8(4)	O(2) – Co(2) – O(2)	180.0(5)
O(4) – W(1) – O(1)	90.1(4)	O(3) – Co(3) – O(3)	119.9(6)
O(5) – W(1) – O(1)	167.0(4)	O(3) – Co(3) – O(3)	104.5(3)
O(6) – W(1) – O(7)	88.8(4)	O(3) – Co(3) – O(3)	104.5(3)
O(4) – W(1) – O(7)	167.3(4)	O(4) – Co(2) – O(6)	93.0(4)
O(5) – W(1) – O(7)	88.3(4)	O(4) – Co(2) – O(6)	93.0(4)
O(1) – W(1) – O(7)	81.5(4)	O(4) – Co(2) – O(6)	87.0(4)
O(6) – W(1) – O(5)	165.6(4)	O(6) – Co(2) – O(6)	180.0(1)
O(4) – W(1) – O(5)	89.5(4)	O(4) – Co(2) – O(2)	91.0(4)
O(5) – W(1) – O(5)	90.2(3)	O(4) – Co(2) – O(2)	89.0(4)
O(1) – W(1) – O(5)	80.0(3)	O(6) – Co(2) – O(2)	90.9(4)
O(7) – W(1) – O(5)	79.6(4)	O(6) – Co(2) – O(2)	89.1(4)
O(4) – Co(2) – O(4)	180.0(1)	O(4) – Co(2) – O(2)	89.0(4)
O(4) – Co(2) – O(6)	87.0(4)	O(3) – Co(3) – O(3)	104.5(3)
O(3) – Co(3) – O(3)	104.5(3)	O(3) – P(5) – O(1)	105.6(5)
O(3) – Co(3) – O(3)	119.9(6)	O(2) – P(5) – O(7)	110.5(5)
O(2) – P(5) – O(3)	113.6(6)	O(3) – P(5) – O(7)	107.5(6)
O(2) – P(5) – O(1)	111.4(5)	O(1) – P(5) – O(7)	107.9(5)

3.3.3.2. Results and Discussion for $(enH_2)_3[Co_3W_4P_4O_{28}]$

The compound $(enH_2)_3[Co_3W_4P_4O_{28}]$ was synthesized by hydrothermal method as blue crystals from the reaction of $Na_2WO_4.2H_2O$, $Co(NO_3)_2.6H_2O$, ethylenediamine and HPO_4.

As a result of single crystal X-ray diffraction analysis, it is obtained that the 3D crystal structure consists of a $[Co_3W_4P_4O_{28}]^{6-}$ anion and three free ethylenediaminium $(N_2H_{10}C_2)^{2+}$ cations.

There are one P atom, one W atom, two Co atoms, seven O atoms and three each C and N atoms which compose the ethylenediaminium cations in 3D structure that is in the asymmetric unit.

The organic components of the structure are present in free position and have disordered structures since the bonds of N atoms with C atoms in ethylenediaminium ions change into two different positions which are shown in Figure 3.19.

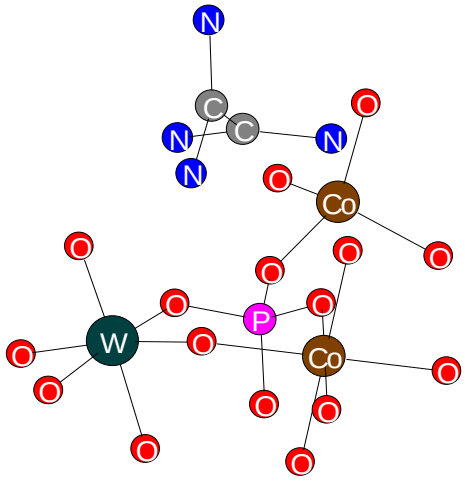

Figure 3.19. The unit structure view of $(enH_2)_3[Co_3W_4P_4O_{28}]$.

In the crystal structure, W atom has an octahedral coordination geometry (WO_6) and P atom has a tetrahedral coordination geometry (PO_4). Therefore, each Co atom has a different coordination geometry. One of these atoms consists of four oxygens, while the other one consists of six oxygens.

As Figure 3.20 illustrates that CoO_6 octahedra connects to four WO_6 octahedra and two PO_4 tetrahedra which are found in trans positions. CoO_4 tetrahedra connects to four PO_4 tetrahedra from the corners. In addition to these, PO_4 tetrahedra has bond with two WO_6, one CoO_6 octahedra and one CoO_4 tetrahedra, while WO_6 octahedra has bonds with two PO_4 tetrahedra, two WO_6 octahedra and two CoO_6 octahedra.

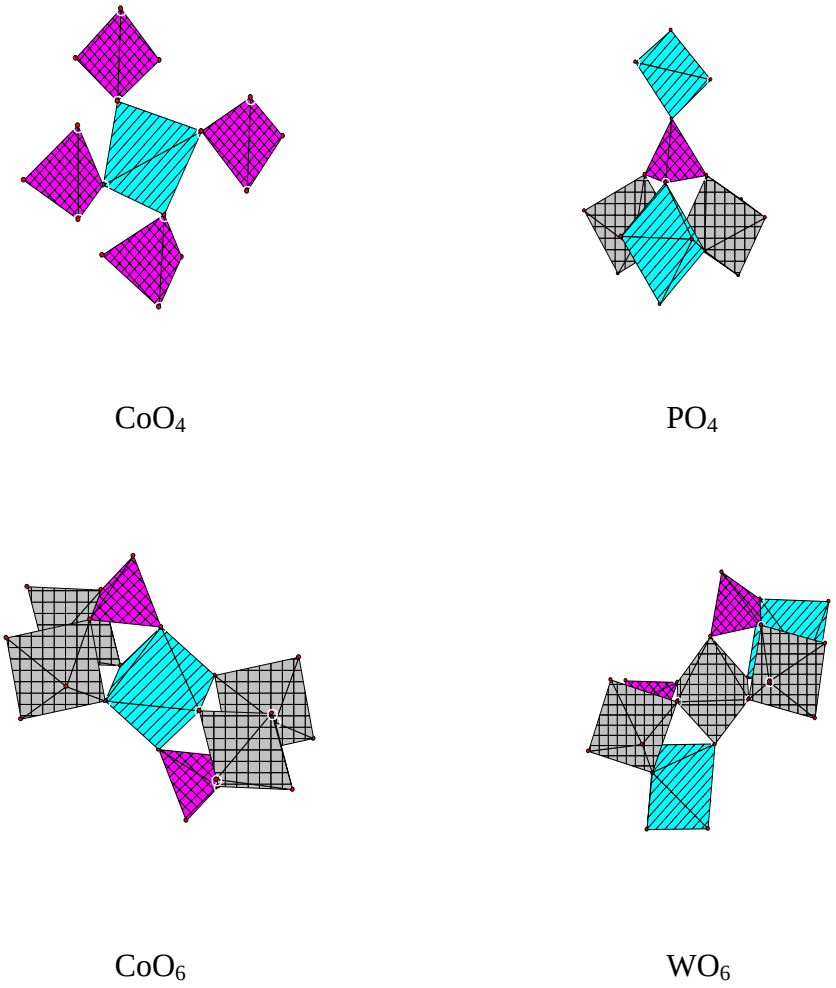

Figure 3.20. The coordinations of Co, P and W polyhedra in $(enH_2)_3[Co_3W_4P_4O_{28}]$.

In $(enH_2)_3[Co_3W_4P_4O_{28}]$ crystal, the groups including four WO_6 octahedra are present between the bonds of cobalt and phosphorus frameworks which are shown in Figure 3.21.

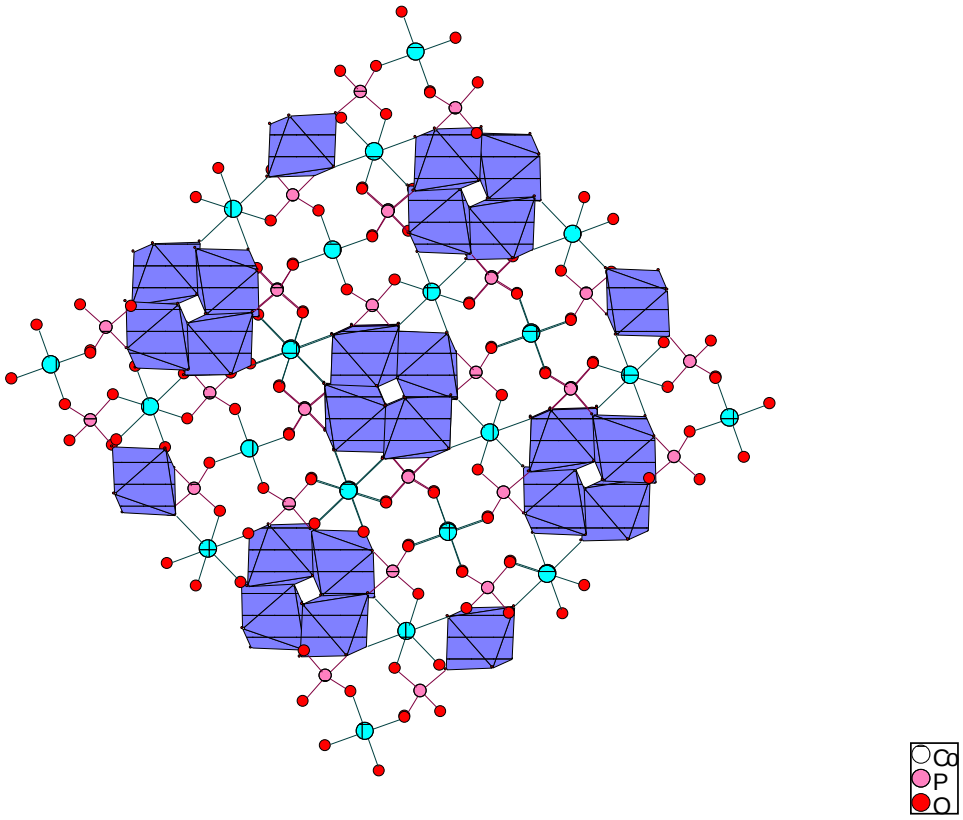

Figure 3.21. The view of $(enH_2)_3[Co_3W_4P_4O_{28}]$ crystal that includes the polyhedral structures.

The W-O bond distances of the crystal are between 1.774(9) and 2.139(9) Å. While the Co-O bond distances of CoO_6 octahedra are between 2.082(9) and 2.113(9) Å, each Co-O bond distance of CoO_4 tetrahedra is 1.936(9) Å. Lastly, the P-O bonds of PO_4 tetrahedra involve distances between 1.522(10)-1.548(9) Å.

The bond valence sums of $(enH_2)_3[Co_3W_4P_4O_{28}]$ shown in Table 3.12 were calculated by Bond Valence Sum, BVS method developed by ID Brown. The results of these calculations show that the oxidation states of W, P, Co and O atoms of the structure are 6+, 5+, 2+ and 2- respectively.

Table 3.12. Bond valence sums of $(enH_2)_3[Co_3W_4P_4O_{28}]$.

	W(1)	P(5)	Co(2)	Co(3)	∑
O(1)	0.649	1.215			1.864
O(2)		1.293	0.642		1.614
O(3)		1.293		0.517	1.810
O(4)	1.472		0.676		1.821
O(5)	1.811				1.811
O(6)	1.472		0.656		1.800
O(7)	0.567	1.205			1.772
∑	5.971	5.006	1.996	2.068	

3.3.4. Synthesis and Characterization of $(4,4'\text{-}bpyH_2)_2(4,4'\text{-}bpyH)[PCoW_{11}O_{39}].H_2O$

$(4,4'\text{-}bpyH_2)_2(4,4'\text{-}bpyH)[PCoW_{11}O_{39}].H_2O$ red crystals were synthesized by using hydrothermal reaction of $Na_2WO_4.2H_2O$ (0.3265 g), $Co(NO_3)_2.6H_2O$ (0.2982 g), 4,4'bipyridine (0.1054 g), 5M H_3PO_4 (2.0 ml) and H_2O (7.0 ml) at 170˚C for 3 days in a 23 ml Teflon-lined autoclave. $Na_2WO_4.2H_2O$ (Sigma-Aldrich, 99%), $Co(NO_3)_2.6H_2O$ (Merck, 99%), 4,4'bipyridine (Alfa Aesar, 98%), H_3PO_4 (Sigma-Aldrich, 85%) were used without further purification.

After all reactants were loaded into the vessel, the mixture was stirred for 20 minutes at laboratory conditions. At the end of stirring, teflon vessel was put into the steel autoclave and heated at 170˚C for 3 days in oven. When the reaction finished, the autoclave was slowly cooled at room temperature. The product was filtered by vacuum filtration and washed several times with pure water. The red crystals were obtained on filter paper by optical microscope. Crystals were characterized by powder X-ray diffraction, FT-IR spectroscopy, SEM-EDX, ICP-MS, single crystal X-ray diffraction, thermogravimetric analysis methods. Elemental analysis by EDX and ICP-MS analysis was performed to confirm the presence of cobalt in the structure. Cobalt atoms were

crystallographically distinguished from W atoms by bond valence analyses of the atoms in question.

$$Na_2WO_4.2H_2O + Co(NO_3)_2.6H_2O + 4,4'\text{-bpy} + H_3PO_4 + H_2O \qquad (3.5)$$
$$0.3265g \qquad 0.2982g \qquad 0.1054g \qquad 2\ ml \qquad 7\ ml$$

$$\xrightarrow[3\ days]{170\ ^\circ C}$$

red crystals

According to the SEM/EDX results of the red crystals shown in Figure 3.22, the compound contains C, N, W, O, P and Co elements in the weight percentages 21.40%, 4.30%, 56.02%, 14.81%, 1.12% and 2.14% respectively.

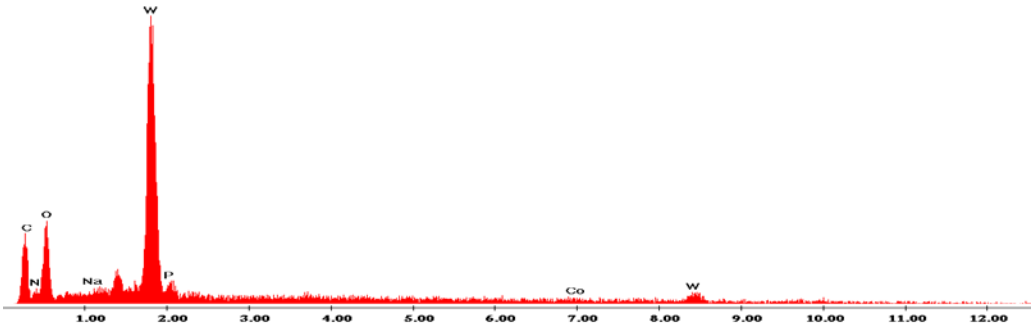

Figure 3.22. SEM/EDX spectrum of $(4,4'\text{-bpyH}_2)_2(4,4'\text{-bpyH})[PCoW_{11}O_{39}].H_2O$.

The synthesized compound was analyzed by powder X-ray diffractometer. The powder pattern of the compound is shown in Figure 3.23. The powder peaks of the compound did not match well with any of the compounds in the XRD database.

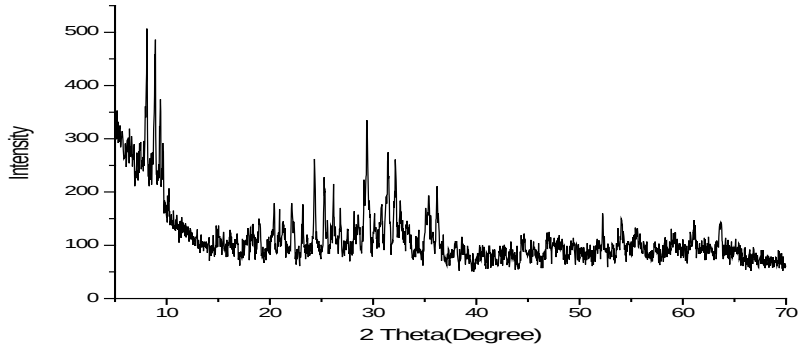

Figure 3.23. XRD spectrum of $(4,4'\text{-bpyH}_2)_2(4,4'\text{-bpyH})[PCoW_{11}O_{39}].H_2O$.

The FT-IR spectrum of $(4,4'\text{-bpyH}_2)_2(4,4'\text{-bpyH})[PCoW_{11}O_{39}].H_2O$ illustrated in Figure 3.24 was recorded in the 4000-450 cm^{-1} region. The peaks in 1200-3200 cm^{-1} can be attributed the characteristic peaks of 4,4'-bipyridine. The peaks in 3000-3200 cm^{-1} range are due to υ(C-H) vibrations, whether the peaks between 1200-1700 cm^{-1} are due to υ(C=C) and υ(C=N) vibrations. The peaks at 1058 and 1075 cm^{-1} are attributed to υ(P-O) vibrations, the peak at 956 cm^{-1} is assigned to υ(W=O) and the peaks between 700-900 cm^{-1} is due to υ(W-O-W) modes. Finally, the peaks at 556 and 589 cm^{-1} are attributed to υ(Co-O) modes.

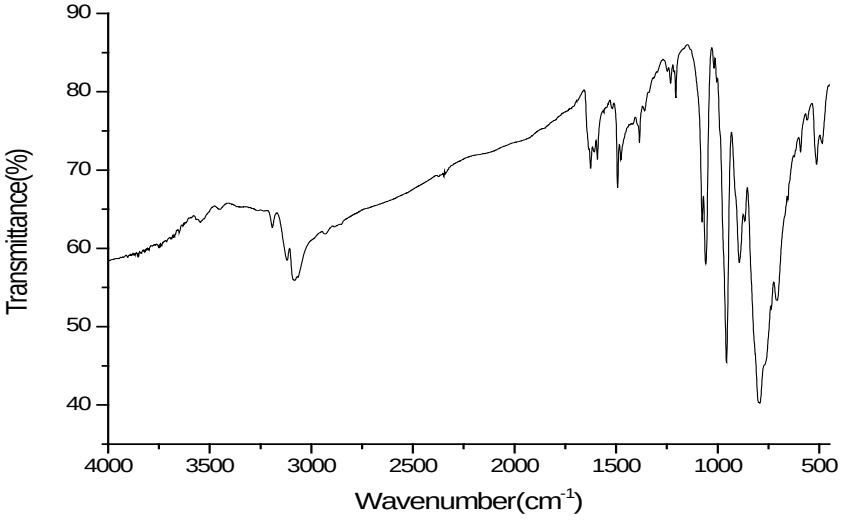

Figure 3.24. FT-IR spectrum of $(4,4'\text{-bpyH}_2)_2(4,4'\text{-bpyH})[PCoW_{11}O_{39}].H_2O$.

The change in the weight of $(4,4'\text{-bpyH}_2)_2(4,4'\text{-bpyH})[PCoW_{11}O_{39}].H_2O$ was measured as a function of temperature and the existence of the organic groups was obtained. The thermogravimetric analysis of the crystal whose graph is illustrated in Figure 3.25 was performed between 30 and 1000˚C in nitrogen atmosphere. The weight extinction until 150˚C is interpreted as the existence of organic impurities and water, whereas the weight extinction (16% w/w) between 150 and 650˚C shows the existence of 4,4'-bipyridine ligands (14% w/w). Therefore, it is illustrated from the graph that the crystal is quite stable at higher temperatures.

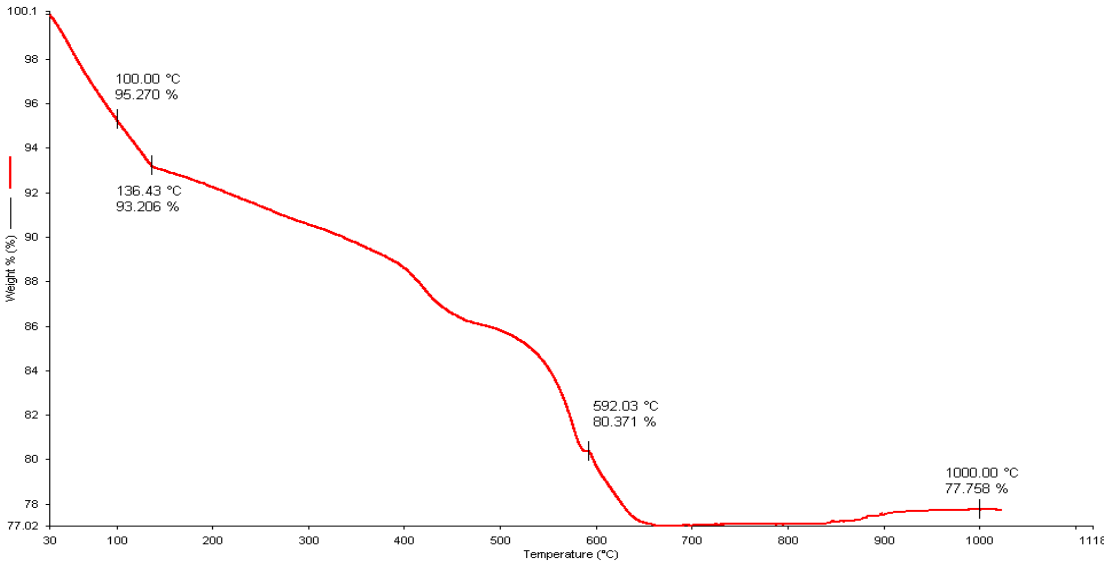

Figure 3.25. TGA graph of $(4,4'\text{-bpyH}_2)_2(4,4'\text{-bpyH})[PCoW_{11}O_{39}].H_2O$.

ICP-MS analysis of $(4,4'\text{-bpyH}_2)_2(4,4'\text{-bpyH})[PCoW_{11}O_{39}].H_2O$ crystal was also performed. The crystals were dissolved in 11 M HNO_3 and then diluted to different concentrations. These diluted solutions were measured and the amount of Co element in the compound was detected. The result of the analysis shows that 1 mg compound involves 373.95 μg Co element.

3.3.4.1. X-ray Crystallographic Analysis of $(4,4'\text{-bpyH}_2)_2(4,4'\text{-bpyH})[PCoW_{11}O_{39}].H_2O$

Single crystal X-ray diffraction of the resulting crystals was performed using a Rigaku AFC8S diffractometer equipped with Mo Kα (λ=0.71073 Å) radiation and a Mercury CCD area detector. Data collection and processing including corrections for absorption and Lorentz and polarization effects were performed using the CrystalClear software package (Version 1.3. Rigaku Corporation, Japan and MSC, The Woodlands, Texas, USA). Candidate space groups were identified based on the systematic absences of the data. The structures were solved by direct methods and refined by full-matrix least squares on F^2 using the SHELXTL software package. All atoms were refined anisotropically in the structures.

Crystallographic data are given in Table 3.13. Selected bond lengths (Å) and bond angles (degree) for $(4,4'\text{-bpyH}_2)_2(4,4'\text{-bpyH})[PCoW_{11}O_{39}].H_2O$ are given in Table 3.14 and Table 3.15 respectively.

Table 3.13. Crystallographic data for $(4,4'\text{-bpyH}_2)_2(4,4'\text{-bpyH})[PCoW_{11}O_{39}].H_2O$.

	(**1**)
Empirical Formula	$PCoW_{11}O_{39}C_{30}N_6H_{24}$
Formula weight	3329.59
Space group	P2(1)/n
a, Å	13.568(3)
b, Å	26.780(5)
c, Å	15.158(3)
α, °	90.00
β, °	100.27(3)
γ, °	90.00
V, $Å^3$	5419.2(19)
Z	4
D_{calc}, Mg/m^3	4.081
Parameters	803
μ, mm^{-1}	25.493
θ range, °	2.6593- 25.05
Reflections	
Collected	36768
Independent	9579
Observed [I≥2σ(I)]	7993
R (int)	0.0782
Final R (obs. data)[a]	
R_1	0.0851
wR_2	0.1951
Final R (all data)	
R_1	0.1018
wR_2	0.2089
Goodness of fit on F^2	1.121
Largest diff. peak, $e/Å^3$	3.180
Largest diff. hole, $e/Å^3$	-8.701

Table 3.14. Selected bond lengths (Å) for $(4,4'\text{-bpyH}_2)_2(4,4'\text{-bpyH})[PCoW_{11}O_{39}].H_2O$.

W(1) – O(36)	1.71(2)	W(10) – O(6)	1.85(2)
W(1) – O(30)	1.90(2)	W(10) – O(30)	1.94(3)
W(2) – O(16)	1.70(2)	W(11) – O(9)	2.01(2)
W(2) – O(15)	1.88(2)	W(11) – O(12)	1.91(2)
W(3) – O(1)	1.95(2)	W(12) – O(17)	1.83(2)
W(3) – O(23)	1.92(2)	W(12) – O(28)	1.96(2)
W(4) – O(26)	1.69(2)	W(1) – O(19)	1.90(2)
W(4) – O(10)	1.81(2)	W(4) – O(5)	1.93(2)
W(5) – O(39)	1.73(2)	W(7) – O(37)	1.97(2)
W(5) – O(13)	1.84(2)	W(8) – O(11)	1.90(2)
W(6) – O(32)	1.68(2)	W(9) – O(24)	1.89(2)
W(6) – O(2)	1.92(2)	W(10) – O(35)	2.42(2)
W(7) – O(38)	1.70(2)	W(3) – O(18)	1.92(2)
W(7) – O(8)	1.83(2)	W(11) – O(33)	2.39(2)
W(8) – O(20)	1.69(2)	W(12) – O(31)	2.39(2)
W(8) – O(25)	1.85(2)	P(1) – O(33)	1.54(2)
W(9) – O(21)	1.687(19)	P(1) – O(31)	1.54(2)
W(9) – O(22)	1.83(2)	P(1) – O(34)	1.55(2)
W(2) – O(29)	1.92(2)	P(1) – O(35)	1.59(2)

Table 3.15. Selected bond angles (°) for $(4,4'\text{-bpyH}_2)_2(4,4'\text{-bpyH})[PCoW_{11}O_{39}].H_2O$.

O(36) – W(1) – O(19)	103.2(10)	O(28) –W(12) – O(6)	159.8(9)
O(30) – W(1) – O(19)	90.1(10)	O(17) –W(12) – O(6)	100.1(9)
O(16) – W(2) – O(15)	103.7(10)	O(33) – P(1) – O(31)	109.7(12)
O(16) – W(2) – O(7)	100.6(11)	O(31) – P(1) – O(34)	109.3(12)
O(9) – W(3) – O(23)	90.4(9)	O(13) – W(5) – O(3)	90.8(11)
O(14) – W(3) – O(18)	101.4(10)	O(39) – W(5) – O(4)	102.7(10)
O(10) – W(4) – O(5)	92.2(10)	O(28) – W(6) – O(2)	90.1(9)
O(26) – W(4) – O(15)	102.4(11)	O(32) – W(6) – O(12)	100.7(12)
O(8) – W(7) – O(2)	87.2(9)	O(21) – W(9) – O(37)	101.7(10)
O(38) – W(7) – O(37)	99.7(10)	O(24) – W(10) – O(30)	88.3(10)
O(35) – W(8) – O(19)	89.2(10)	O(27) – W(10) – O(29)	100.0(10)
O(20) – W(8) – O(11)	99.3(12)	O(12) – W(11) – O(8)	88.0(9)
O(22) – W(9) – O(24)	87.7(10)	O(17) – W(11) – O(13)	100.1(9)

3.3.4.2. Results and Discussion for $(4,4'\text{-bpyH}_2)_2(4,4'\text{-bpyH})[PCoW_{11}O_{39}].H_2O$

The crystal $(4,4'\text{-bpyH}_2)_2(4,4'\text{-bpyH})[PCoW_{11}O_{39}].H_2O$ was synthesized with using hydrothermal method from the reaction of $Na_2WO_4.2H_2O$, $Co(NO_3)_2.6H_2O$, 4,4'-bipyridine and H_3PO_4.

As a result of single crystal X-ray diffraction, it is obtained that the structure includes $[PCoW_{11}O_{39}]^{5-}$ Keggin polyanion clusters, 4,4'-bipyridine ligands and water molecules. Keggin polyanion cluster consists of 12 edge-and-corner sharing WO_6 octahedra and there is a PO_4 tetrahedra at the center that is illustrated in Figure 3.26. $[PCoW_{11}O_{39}]^{5-}$ polyanion cluster shares its one oxygen with another $[PCoW_{11}O_{39}]^{5-}$ polyanion cluster and forms the chain structure that is shown in Figure 3.27. The chain structures and water molecules have C-H…O hydrogen bond interactions between eachother.

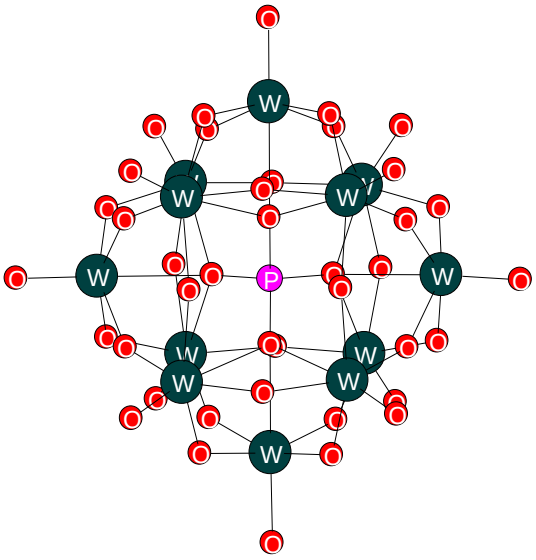

Figure 3.26. The view of $[PCoW_{11}O_{39}]^{5-}$ Keggin polyanion cluster.

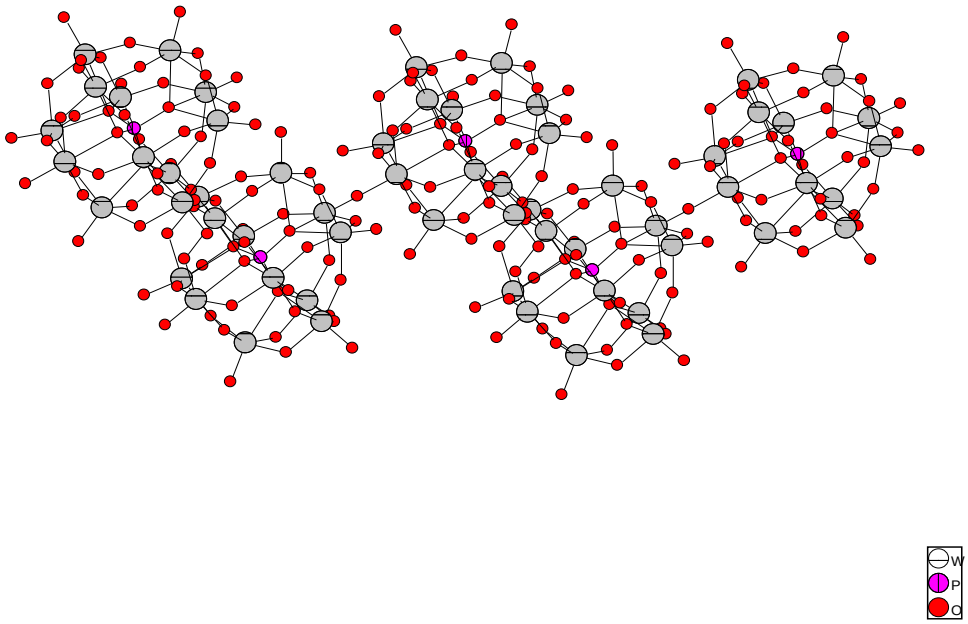

Figure 3.27. The chain structure of $[PCoW_{11}O_{39}]^{5-}$ Keggin polyanions.

In the unitcell that is shown in Figure 3.28, there are four polyanion clusters and 4,4'-bipyridine ligands among these clusters. WO_6 octahedral structures involve three different W-O bonds. These are; W-Ot (terminal) bonds whose distances range from 1.68(2) to 1.73(2) Å which indicates a W=O multiple bond, W-Ob (bridging) bonds whose distances range from 1.85(2) to 2.01(2) Å and W-Oc (central) bonds range from 2.39(2) to 2.47(2) Å respectively. Therefore, the distances of P-O bond distances are between 1.54(2) and 1.59(2) Å.

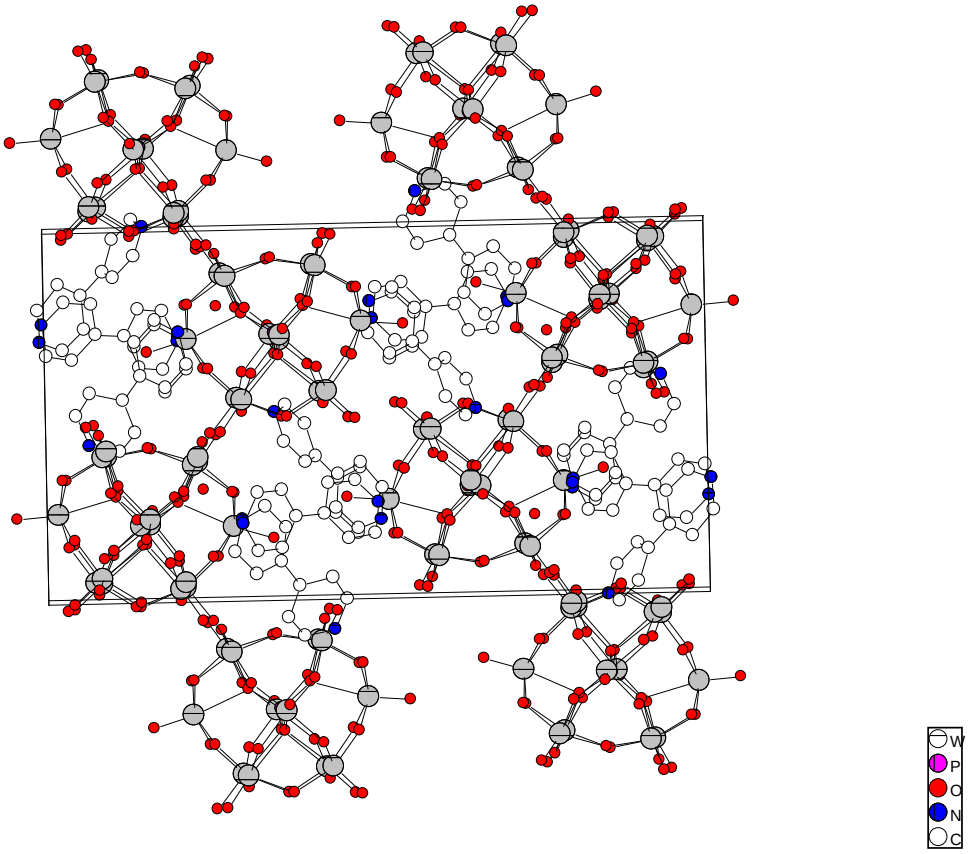

Figure 3.28. The unitcell view of $(4,4'\text{-bpyH}_2)_2(4,4'\text{-bpyH})[PCoW_{11}O_{39}].H_2O$.

The bond valence sums of $(4,4'\text{-bpyH}_2)_2(4,4'\text{-bpyH})[PCoW_{11}O_{39}].H_2O$ shown in Table 3.16 were calculated by Bond Valence Sum, BVS method developed by ID Brown. The results of these calculations show that, the oxidation states of W, P, O and Co atoms of the structure are 6+, 5+, 2- and 2+ respectively. Only the valence sums of W(11) and W(12) are 4.988 and 4.935 alternately and these atoms share the same position with Co(11) and Co(12). These cobalt atoms are in the same crystallographic position with 50% occupancy factor. The compound needs 5+ valence cations and they are provided by 4,4'-bipyridine ligands. These ligands change into 4,4'-$bpyH_2^{2+}$ cation and 4,4'-$bpyH_2^{\bullet+}$ radical cation easily in acidic medium. It is thought that, the organic part of the synthesized material includes bipyridinium cation and bipyridinium radical cation.

Table 3.16. Bond valence sums of $(4,4'\text{-bpyH}_2)_2(4,4'\text{-bpyH})[PCoW_{11}O_{39}].H_2O$.

	W(1)	W(2)	W(3)	W(4)	W(5)	W(6)	W(7)	W(8)	W(9)	W(10)	W(11)	W(12)	Co(11)	Co(12)	P(1)	∑
O(1)		0.992	0.915													1.907
O(2)						0.992	1.019									2.011
O(3)					1.047			0.940								1.987
O(4)	0.965				0.940											1.905
O(5)				0.965		0.965										1.930
O(6)										1.199		0.843		0.448		1.962
O(7)	0.940	1.019														1.959
O(8)							1.265				0.915		0.506			2.180
O(9)			1.105								0.778		0.385			1.883
O(10)				1.335								0.790		0.408		2.125
O(11)							0.867	1.047								1.914
O(12)						0.965					1.019		0.538			1.984
O(13)					1.231						0.799		0.433			2.030
O(14)			1.750													1.750
O(15)		1.105		0.965												2.070
O(16)		1.798														1.798
O(17)											1.199	1.265	0.632	0.686		2.464
O(18)			0.992		0.915											1.907
O(19)	1.047							1.105								2.152
O(20)								1.847								1.847

(cont. on the next page)

Table 3.16. (cont.)

O(21)									1.862							1.862
O(22)									1.265			0.869		0.455		2.134
O(23)			0.992	0.867												1.859
O(24)									1.076	1.019						2.095
O(25)								1.199	0.821							2.020
O(26)				1.847												1.690
O(27)										1.847						1.847
O(28)						1.047						0.890		0.485		1.937
O(29)		0.992								0.940						1.932
O(30)	1.047									0.940						1.987
O(31)				0.264		0.237						0.278			1.231	2.010
O(32)						1.898										1.898
O(33)			0.257		0.224						0.278				1.231	1.990
O(34)							0.257	0.224	0.237						1.199	1.917
O(35)	0.243	0.271								0.257					1.076	1.847
O(36)	1.750															1.750
O(37)							0.867		1.019							1.886
O(38)							1.798									1.798
O(39)					1.658											1.658
∑	5.992	6.177	6.011	6.243	6.015	6.104	6.073	6.362	6.280	6.202	4.988	4.935	2.494	2.482	4.737	

CHAPTER 4

CONCLUSION

In this thesis; hydrothermal synthesis and structural characterization of open-framework metal phosphates templated with organic diamines were studied. Vanadium and tungsten transition metals were used to build up the inorganic framework, 4,4'-bipyridine and ethylenediamine were used as the organic ligands of the hybrid materials. At the end of the hybrid reactions, several crystals were synthesized and they were characterized by using different techniques. These techniques are; powder X-ray diffraction, optical microscopy, scanning electron microscopy (SEM), fouier transform infrared spectroscopy (FT-IR), inductively coupled plasma/mass spectrometry (ICP-MS) and thermogravimetric analysis. The compounds discussed in this study, involve a novel and three known materials whose structures were solved by SHELXTL program.

The synthesized novel compound is $(4,4'\text{-bpyH}_2)_2(4,4'\text{-bpyH})[PCoW_{11}O_{39}].H_2O$ red crystals. The red crystals were synthesized by using the hydrothermal reaction of $Na_2WO_4.2H_2O$, $Co(NO_3)_2.6H_2O$, 4,4'-bipyridine and H_3PO_4 in a Teflon-lined autoclave at 170˚C for 3 days. The compound cystallizes in the space group P2(1)/n of the monoclinic system with four formula units in a cell with dimensions a=13.568(3) Å, b=26.780(5) Å, c=15.158(3) Å and its volume is 5419.2(19) $Å^3$. The crystal consists of Keggin polyoxometalate clusters which include WO_6 octahedra and a PO_4 tetrahedron at the center. The 1-D chains of the crystal are formed by one oxygen sharing $[PCoW_{11}O_{39}]^-$ clusters and 4,4'-bipyridinium organic groups and H_2O exist between the chains through hydrogen bonding interactions.

One of the known compounds that was synthesized hydrothermally is $Co(4,4'\text{-bpy})_2(VO_2)_2(HPO_4)_2$ red columnar crystals. These red crystals were obtained from the reaction of $Na_2WO_4.2H_2O$, $NaVO_3$, $Co(NO_3)_2.6H_2O$, 4,4'-bipyridine and H_3PO_4 at 170 ˚C for 3 days. The compound crystallizes in the space group C2/c of the monoclinic system with four formula units in a cell with dimensions a=25.1790(5) Å, b=8.1257(16) Å, c=15.6403(3) Å and volume is 2544.9(9) $Å^3$. The crystal consists of $[(VO_2)(HPO_4)]_\infty$ helical chains and $[Co(4,4'\text{-bpy})_2]^{2+}$ frameworks.

The other known compound $NaCo_3(PO_4)(HPO_4)_2$ pink rod-like crystals were synthesized by the hydrothermal reaction of $Na_2WO_4.2H_2O$, $NaVO_3$, $Co(NO_3)_2.6H_2O$, 4,4'-bipyridine and HPO_4 at 170˚C for 3 days. The compound crystallizes in the space group C2/c of the monoclinic system with four formula units in a cell with dimensions a=11.872(2) Å, b=12.150(2) Å, c=6.5107(13) Å and its volume is 857.5(3) $Å^3$. CoO_6 octahedra in the structure form chains by corner sharing and these chain structures connect to the PO_4 and HPO_4 groups and build up adjacent layers.

The last known compound $(enH_2)_3[CoW_4P_4O_{28}]$ was synthesized as octahedral dark blue crystals from the hydrothermal reaction of $Na_2WO_4.2H_2O$, $Co(NO_3)_2.6H_2O$, ethylenediamine and HPO_4 at 170˚C for 3 days. The compound crystallizes in the space group I4(1)/a of the tetragonal system with four formula units in a cell with dimensions a=17.138(2) Å, b=17.138(2) Å, c=10.775(3) Å and its volume is 3164.6(9) $Å^3$. The crystal consists of a $[Co_3W_4P_4O_{28}]^{6-}$ anion and three free ethylenediaminium cations.

In conclusion, many products were synthesized hydrothermally at the end of several experiments. The most significant compounds were discussed here. According to the results, it is possible to synthesize different organic-inorganic hybrid materials in glamorous crystalline form by changing the components and using the hydrothermal technique.

REFERENCES

Boudin, S.; Guesdon, A.; Leclaire, A.; Borel, M. M. Review on vanadium phosphates with mono anddivalent metallic cations: syntheses, structural relationships and classification, properties. *International Journal of Inorganic Materials.* **2000**, *2*(6), 561-579.

Byrappa, K.; Yoshimura, M. *Handbook of hydrothermal technology: A technology for crystal growth and materials processing*. William Andrew: New York, 2001.

Casañ-Pastor, N.; Gómez-Romero, P. Polyoxometalates: from inorganic chemistry to materials science. *Frontiers in Bioscience.* **2004**, *9*, 1759-1770.

Eral, L. Hydrothermal synthesis and characterization of transition metal (Mn and V) oxides containing phosphates. MSc thesis, İzmir Institute of Technology, İzmir, June 2006.

Gallegos, A. K. C. Organic/inorganic hybrid materials based on conducting organic polymers as electrodes for energy storage devices. PhD thesis, Materials Science Institute of Barcelona, 2003.

Gao, S.; Li, T.; Lü, J.; Cao, R. Two novel grid networks based on Keggin-type polyoxometalate clusters assembled through weak Cu··O interactions. *Inorganic Chemistry Communications.* **2007**, *10*(5), 551-554.

Goldstein, J. *Scanning electron microscopy and X-ray microanalysis*. Springer Us, 2003; Vol. 1.

Hagrman, P. J.; Hagrman, D.; Zubieta, J. Organic-inorganic hybrid materials: From simple coordination polymers to organodiamine-templated molybdenum oxides. *Angewandte Chemie-International Edition.* **1999**, *38*, 2639-2684.

Hayashi, H.; Hakuta, Y. Hydrothermal Synthesis of Metal Oxide Nanoparticles in Supercritical Water. *Materials.* **2010**, *3*(7), 3794-3817.

Kaul, E. E. *Experimental investigation of new low-dimensional spin systems in vanadium oxides*. Dresden, 2005.

Kepenekci, O.; Emirdag-Eanes, M.; Demir, M. M.. Effect of Alkali Metal Hydroxides on the Morphological Development and Optical Properties of Ceria Nanocubes Under Hydrothermal Conditions. *Journal of Nanoscience and Nanotechnology.* **2011**, *11*(4), 3565-3577.

Kickelbick, G. *Introduction to hybrid materials*. John Wiley & Sons: England, 2007.

Kozhevnikov, I. *Catalysis by polyoxometalates*. John Wiley & Sons: England, 2002.

Li, G.; Ding, Y.; Wang, J.; Wang, X.; Suo, J. New progress of Keggin and Wells–Dawson type polyoxometalates catalyze acid and oxidative reactions. *Journal of Molecular Catalysis.* **2007**, *262*(1-2), 67-76.

Liu, J.; Xu, M.; Wang, E. B. A new extended structural compound based on saturated Wells–Dawson polyoxoanions. *Chinese Chemical Letters.* **2009**, *20*, 1381-1385.

Rajeswari, J.; Kishore, P. S.; Viswanathan, B.; Varadarajan, T. K.. Facile Hydrogen Evolution Reaction on WO_3 Nanorods. *Nanoscale Research Letters.* **2007**, *2*(10), 496-503.

Rao, C. N. R.; Natarajan, S.; Choudhury, A.; Neeraj, S.; Ayi, A. A. Aufbau Principle of Complex Open-Framework Structures of Metal Phosphates with Different Dimensionalities. *Accounts of Chemical Research.* **2001**, *34*, 80-87.

Schubert, U.; Hüsing, N. *Synthesis of inorganic materials*. Wiley-VCH: Weinheim, 2005.

Sha, J.; Peng, J.; Liu, H.; Xue, B.; Chen, J.; Tian, A.; Zhang, P. Controlled assembly of two novel 3D hexad-supporting Keggin-polyoxometalate derivatives: {[Cu(4,4′-bipy)]$_3$[HnX$W_{12}O_{40}$]}[4,4′-bipy]·2H_2O (X=P, n=0; X=Si, n=1). *Journal of Molecular Structure.* **2007**, *871*(1-3), 85-91.

Smart, L.; Moore, E. A. *Solid state chemistry: An introduction*. Taylor & Francis: New York, 2005.

Taylor, H. E. *Inductively coupled plasma-mass spectrometry: practices and techniques*. Academic Pr, 2001.

West, A. R. *Solid State Chemistry and its Applications*. John Wiley & Sons: England, 1984.

Xu, R.; Pang, W.; Huo, Q. *Modern Inorganic Synthetic Chemistry*. Elsevier, 2010.

Zamanian, A.; Hardiman, C. Electromagnetic Radiation and Human Health: A Review of Sources and Effects. *High Frequency Electronics.* **2005**, *16*, 16-26.